이학박사 학위논문

골지체 스트레스에서 비자가포식적 LC3 단백질 지질화의 분자 기전 및 기능에 관한 연구

Studies on the molecular mechanism and function of non-autophagic LC3 lipidation under Golgi stress

2025 년 2 월

서울대학교 대학원

생명과학부

강 재 민

골지체 스트레스에서 비자가포식적 LC3 단백질 지질화의 분자 기전 및 기능에 관한 연구

지도교수 정 용 근

이 논문을 이학박사 학위논문으로 제출함
2024 년 11 월

서울대학교 대학원
생명과학부
강 재 민

강재민의 이학박사 학위논문을 인준함
2024 년 11 월

위 원 장 허 원 기 (인)

부위원장 정 용 근 (인)

위 원 박 상 현 (인)

위 원 이 진 아 (인)

위 원 장 원 열 (인)

Abstract

Studies on the molecular mechanism and function of non-autophagic LC3 lipidation under Golgi stress

Jaemin Kang

School of Biological Sciences

The Graduate School

Seoul National University

Lipidated ATG8/LC3 proteins are recruited to single membrane compartments, such as endosomes and lysosomes, as well as double-membraned autophagosomes to support their functions. Although recent studies have shown that LC3 lipidation occurs on the Golgi apparatus membranes following several Golgi-damaging

conditions, molecular mechanism and biological function of Golgi-LC3 lipidation remain unknown.

Here, I established DLK1 overexpression as a new strategy for studying Golgi-specific LC3 lipidation. Combining this with Golgi-damaging reagents, niclosamide and AMDE-1, I unravel the mechanism and role of Golgi-LC3 lipidation. I found that upon DLK1 overexpression, the *trans*-Golgi network is lipidated by LC3 via ATG12-ATG5-ATG16L1 complex, two ubiquitin-like conjugation systems in autophagy. Upstream autophagy regulators including ULK1/2 and FIP200 are dispensable for DLK1-induced LC3 lipidation. I confirmed that post-Golgi trafficking blockade is the primary cause of Golgi-LC3 lipidation under DLK1 overexpression and niclosamide/AMDE-1 incubation. Golgi-LC3 lipidation requires ATG16L1 recruitment to the Golgi apparatus which is mediated through interaction between ATG16L1 WD40 domain and V-ATPase. During post-Golgi trafficking inhibition, TFE3, one of the key transcriptional regulators of the Golgi stress response, is translocated to the nucleus and upregulates Golgi stress response target genes. Defects in LC3 lipidation impair TFE3 nuclear translocation specifically under Golgi dysfuction, leading to dysregulation of the Golgi stress response. Taken together, this study demonstrates the mechanism and novel function of Golgi-LC3 lipidation in the Golgi stress response.

Key words: Golgi apparatus, LC3 lipidation, DLK1, Post-Golgi trafficking, V-ATPase, Golgi stress response

Student Number: 2016-20373

Table of Contents

List of Figures

Introduction

Non-autophagic ATG8/LC3 lipidation on single membranes

In autophagy, ATG8 (mammalian LC3/GABARAPs, hereafter LC3), one of the key regulators of autophagy process, is conjugated to phosphatidylethanolamine (PE), which is essential for localization of cytosolic protein LC3 to membrane of autophagosomes (Ichimura et al, 2000; Kabeya et al, 2000). The LC3 lipidation process is mediated by two ubiquitin-like conjugation systems in which ATG12 and LC3 are conjugated to ATG5 and phospholipid, respectively (Mizushima, 2020). ATG7 and ATG10 mediate ATG12-ATG5 conjugation to generate ATG12-ATG5-ATG16L1 complex. After LC3-I generation by ATG4-mediated proteolytic cleavage of LC3, ATG12-ATG5-ATG16L1 complex together with ATG7 and ATG3 conjugates LC3-I to phospholipid to form membrane-bound LC3-II.

In addition to double membrane-structured autophagosomes, LC3 also can be recruited to several single membrane structures such as endosomes and lysosomes (Heckmann et al, 2019; Sanjuan et al, 2007; Sønder et al, 2021), known as conjugation of ATG8/LC3 to single membranes (CASM). CASM has distinct molecular mechanism separate from autophagic LC3 lipidation (Durgan & Florey, 2022). CASM does not require most of the upstream autophagy regulators including ULK1/2, FIP200, ATG9, WIPI2 and ATG14L. The V-ATPase-ATG16L1 axis is a prominent feature of

CASM. V1 subunit of V-ATPase binds to WD40 domain of ATG16L1, which domain is dispensable for autophagy and absent in yeast homolog Atg16 (Mizushima et al, 2003), for ATG16L1 recruitment to single membrane structures (Fischer et al, 2020; Fletcher et al, 2018; Xu et al, 2019). In autophagy, V-ATPase inhibitors, such as bafilomycin A1 (Baf.A1) and concanamycin A (ConA), increase LC3-II protein levels as those inhibitors block lysosomal degradation of LC3 proteins via lysosomal neutralization (Klionsky et al, 2021). In CASM, however, V-ATPase inhibitors rather decrease LC3-II protein levels via dissociation of V0-V1 subunits, followed by disruption of V-ATPase-ATG16L1 interaction and LC3 delipidation (Hooper et al, 2022; Ulferts et al, 2021). Compared to PE-specific conjugation on autophagosomes, LC3 can be conjugated to both PE and phosphatidylserine (PS) in CASM (Durgan et al, 2021).

Autophagic LC3 lipidation functions in diverse steps of autophagy process from initiation of autophagosome formation to late step of autophagy including autophagosome closure, autophagosome-lysosome fusion and autophagosomal inner membrane degradation (Mizushima, 2020). In CASM, LC3 lipidation supports the functions of various single-membraned organelles such as phagosomes, endosomes, macropinosomes and lysosomes (Durgan & Florey, 2022; Leidal et al, 2020; Nakamura et al, 2020). In LC3-associated phagocytosis, LC3 lipidation on the outer face of phagosomes facilitates phagosome-lysosome fusion (Peña-

Martinez et al, 2022). LC3 supports fusion of single-membraned entotic vacuoles and macropinosomes to lysosomes (Florey et al, 2011). LC3 lipidation also facilitates non-degradative function of organelles; extracellular vesicles cargo loading and secretion (Leidal et al., 2020), β-amyloid receptor recycling via LC3-associated endocytosis (Heckmann et al, 2019) and TFEB activation under lysosomal damage (Nakamura et al., 2020).

Golgi-LC3 lipidation induced by Golgi damages

Recent studies have shown that chemical reagents (niclosamide and AMDE-1, autophagy modulator with dual effects), fatty acid oleate and several Golgi-damaging strategies induce LC3 lipidation on the Golgi apparatus (Cerrato et al, 2021; Gao et al, 2016; Gomes-da-Silva et al, 2019; Liu et al, 2019). Niclosamide and AMDE-1 induce LC3 lipidation in a manner that is independent of ULK1, FIP200, Beclin 1 and WIPI2, but dependent on two ubiquitin-like conjugation systems (Gao et al, 2016; Liu et al, 2019). Niclosamide/AMDE-1-induced LC3 lipidation requires intact Golgi apparatus structure and is abrogated by V-ATPase inhibitors. Various Golgi-damaging strategies, including laser irradiation, local production of polybenzimidazole, photodynamic therapy and Golgi disruption by LTX-401, recruit LC3 to Golgi-associated single membranes via ATG12-ATG5-ATG16L1 complex (Gomes-da-Silva et al, 2019). This LC3 recruitment is inhibited by V-ATPase inhibitors. Additionally, loss of ATG5 and ATG7 exacerbates Golgi

damage-induced cell death, suggesting cytoprotective function of LC3 lipidation. Oleate, an endogenous *cis*-unsaturated fatty acid, accumulates LC3 on the *trans*-Golgi network via Beclin 1 complex-independent manner (Cerrato et al, 2021). Role of V-ATPase in oleate-induced LC3 lipidation is not yet defined.

Collectively, Golgi-LC3 lipidation from various Golgi-damaging conditions commonly shows unique features of CASM, disengagement of upstream autophagy regulators and suppression by V-ATPase inhibitors. However, compared to LC3 lipidation on phagosomes and endolysosomes, little is known about the process of Golgi-LC3 lipidation. The mechanism by which various Golgi-damaging conditions commonly lead to LC3 lipidation and the role of LC3 lipidation against Golgi apparatus damage need to be elucidated.

Golgi apparatus quality control by proteasomes and lysosomes

The Golgi apparatus operates as a central hub for modification and intracellular transport of proteins and lipids (Viotti, 2016). Structural or functional disruption of the Golgi apparatus induces Golgi stress, and then adaptive cellular responses are accompanied to restore Golgi homeostasis (Kim et al, 2023; Schwabl & Teis, 2022).

Similar to mitochondria and endoplasmic reticulum (ER), Golgi apparatus quality control could be maintained by proteasomal and lysosomal degradation pathways (Benyair et al, 2022; Chang &

Yang, 2022; Schwabl & Teis, 2022). Golgi apparatus membrane-associated 26S proteasomes degrade GM130 for Golgi dispersal under Golgi stress to facilitate Golgi apparatus-related degradation (GARD) (Eisenberg-Lerner et al, 2020). Analogous to ER-associated degradation (ERAD) pathway, endosome and Golgi-associated degradation (EGAD) pathway degrades endosome and Golgi membrane proteins by cytosolic proteasomes to regulate proteostasis and lipid homeostasis (Schmidt et al, 2019). In Golgi membrane-associated degradation (GOMED), Golgi and cytoplasmic components are engulfed in Golgi-derived double-membraned vesicles, followed by lysosomal degradation (Yamaguchi et al, 2016). Golgi-phagy receptors, YIPF3/4 and CALCOCO1, were recently shown to engage in selective degradation of the Golgi apparatus under nutrient stress (Hickey et al, 2023; Nthiga et al, 2021). It has not yet been determined whether Golgi-LC3 lipidation is related to proteasome or lysosome-mediated Golgi quality control. Since Golgi-LC3 lipidation induced by polybenzimidazole and AMDE-1 occurs in single membranes rather than autophagosomes (Gao et al., 2016; Gomes-da-Silva et al., 2019), it is unlikely to be associated with Golgi-phagy. Considering the function of LC3 in LC3-associated phagocytosis and micropinocytosis, it is also necessary to investigate whether Golgi-LC3 lipidation plays a role in the fusion between Golgi-derived vesicles and lysosomes.

Golgi stress response for Golgi homeostasis

In response to Golgi stress induced by insufficient Golgi function, transcription of genes related to Golgi homeostasis or cell death is induced, which is referred to as the 'Golgi stress response' (Gao et al, 2021; Kim et al, 2023; Taniguchi & Yoshida, 2017). Similar to mitochondrial, ER and lysosomal stress responses, Golgi stress response consists of four key components; a sensor that perceives Golgi stress, a transcription factor that regulates transcription of genes related to Golgi function, an enhancer element where transcription factor binds; and target genes (Taniguchi & Yoshida, 2017). Golgi stress response pathways are composed of transcription factor binding to IGHM enhancer 3 (TFE3), heat shock protein 47 (HSP47), CAMP responsive element binding protein 3 (CREB3), mitogen-activated protein kinases-erythroblast transformation specific (MAPK-ETS), proteoglycan and mucin pathways (Kim et al., 2023). TFE3, a member of the MiT family of the bHLH-leucine zipper transcription factor, regulates cellular adaptive response against various types of organelle stress via translocation from the cytosol to the nucleus after dephosphorylation (Martina et al, 2016; Martina et al, 2014; Nezich et al, 2015; Roczniak-Ferguson et al, 2012). Under Golgi stress, TFE3 also translocates to the nucleus and binds to the Golgi apparatus stress response element (GASE) for transcriptional activation of genes related to Golgi function including glycosylation, Golgi structure and vesicle transport (Taniguchi et al, 2015). O-

glycosylation inhibition induces mRNA expression of ER-resident chaperone HSP47 and HSP47 inhibits cell death (Miyata et al, 2013). Golgi stress induced by brefeldin A, golgicide A, Exo1 and monensin activates CREB3 and MAPK-ETS (Baumann et al, 2018; Reiling et al, 2013). CREB3 is cleaved and translocated to the nucleus for expression of pro-apoptotic gene ARF4 (Raggo et al, 2002; Reiling et al., 2013). In MAPK-ETS pathway, activation of MEK1/2 and ERK1/2 enhances activity of ETS family transcription factors to induce apoptosis under Golgi stress (Baumann et al., 2018). Insufficient glycosylation of proteoglycan and mucin upregulates genes of glycosylation enzymes through the unidentified transcription factors (Jamaludin et al, 2019; Sasaki et al, 2019). Precise molecular mechanisms of those Golgi stress response pathways remain unclear. Sensor molecules and sensing mechanism of most pathways have not been elucidated. Even in the HSP47, proteoglycan and mucin pathways, the transcription factors have not yet been identified. In TFE3 pathway, while calcineurin and protein phosphatase 2A have been identified as TFE3 phosphatase under nutrient, ER and oxidative stress conditions (Martina et al., 2016; Martina & Puertollano, 2018), the kinase and phosphatase that regulate TFE3 phosphorylation specifically under Golgi stress has yet to be identified.

In case of TFEB, another member of MiT family of the bHLH-leucine transcription factor together with TFE3, its nuclear translocation is regulated by ATG8 family proteins in several

cellular stress conditions (Goodwin et al, 2021; Kumar et al, 2020; Nakamura et al., 2020). Under lysosomal damage, LC3 is lipidated on lysosomal membranes and facilitates TFEB nuclear translocation via interaction with the lysosomal calcium channel TRPML1 (Nakamura et al., 2020). GABARAP-mediated sequestration of FLCN-FNIP tumor suppressor complex is required for TFEB activation in parkin-dependent mitophagy, Salmonella infection and endolysosomal ion imbalance (Goodwin et al., 2021). GABARAP and GABARAPL1, together with their interactor IRGM, regulate TFEB activation under nutrient stress and pathogen infection (Kumar et al., 2020). Similar to TFEB, it should be examined whether LC3 lipidation could regulate TFE3 activity under Golgi stress conditions.

In the present study, I demonstrate that ectopic expression of DLK1 induces non-autophagic Golgi-LC3 lipidation which requires two ubiquitin-like conjugation systems. Comparing with niclosamide and AMDE-1, I reveal a common mechanism of Golgi-LC3 lipidation. Both DLK1 overexpression and Golgi-damaging reagents inhibit post-Golgi trafficking and recruit ATG16L1 to the Golgi apparatus by V-ATPase. I further demonstrate novel function of Golgi-LC3 lipidation in that LC3 facilitates TFE3-mediated Golgi stress response to restore Golgi homeostasis.

Results

Overexpression of DLK1 accumulates LC3 on the *trans*-Golgi network

I first performed a gain-of-function screening process using cDNA expression library encoding membrane proteins to identify an autophagy regulator. Unexpectedly, I found that overexpression of DLK1 induced unusual intracellular LC3B accumulation in HeLa cells (Figure 1. A, B). DLK1, a non-canonical NOTCH ligand composed of six tandem EGF-like repeats and single transmembrane domain, inhibits NOTCH signaling via EGF repeats and has various roles in development, adipogenesis and tumourigenesis (Baladrón et al, 2005; Falix et al, 2012; Grassi & Pietras, 2022; Smas et al, 1994). As DLK1 is known to be transported to the plasma membrane through the Golgi apparatus or be secreted (Macedo & Kaiser, 2019), I hypothesized that the overexpressed DLK1 might recruit LC3B to the Golgi apparatus. Unlike RFP-LC3B distributed in the control cytoplasm, RFP-LC3B highly colocalized with the *trans*-Golgi network membrane protein TGOLN2 (also known as TGN46) upon DLK1 overexpression (Figure 1. A). On the other hand, LC3B did not colocalize with the

cis-Golgi protein GM130 under the same condition (Figure 1. B). Intriguingly, immunoblot analysis showed that DLK1 overexpression increased the conversion of LC3B-I to LC3B-II (Figure 1. C). However, transmission electron microscopy analysis revealed no accumulation of double-membraned autophagosomes on the trans-Golgi network (Figure 2.). In contrast to DLK1, overexpression of canonical NOTCH ligand DLL1 and DLL3, structure of which are similar to DLK1 (D'Souza et al, 2010), neither accumulated GFP-LC3B (Figure 3. A) nor induced GFP-LC3B-II conversion (Figure 3. B), demonstrating DLK1-specific LC3 accumulation. Mammalian LC3 proteins (LC3A, LC3B and LC3C) and GABARAP proteins (GABARAP, GABARAPL1 and GABARAPL2) were all recruited onto the *trans*-Golgi network upon DLK1 overexpression (Figure 4.). These data suggest that DLK1 overexpression recruits ATG8 proteins onto the *trans*-Golgi network.

DLK1 isoform 2 does not induce LC3 accumulation on the Golgi apparatus

To examine how DLK1 recruits LC3 onto the *trans*-Golgi network, I decided to characterize which region of DLK1 is required for LC3 accumulation. Serial deletion mutants (Δ) of DLK1 lacking one of

the six tandem EGF-like repeats or a cleavage domain and DLK1 isoform 2 lacking region spanning residue 229 to 301 were generated (Figure 5. A). Among them, overexpression of EGF 4-lacking DLK1 mutant and DLK1 isoform 2 was unable to induce LC3B accumulation (Figure 5. B) and LC3B-II conversion in HeLa cells (Figure 5. C). When I examined subcellular localization, immunostaining of DLK1 confirmed that DLK1 WT and isoform 2 localized to the *trans*-Golgi network (Figure 6.). However, DLK1 mutant lacking EGF-like repeat 4 was found in the ER, suggesting that inability of this mutant to accumulate LC3 is due to its inappropriate localization (Figure 6.). These results related to isoform 2 indicate that a luminal region near the transmembrane domain (TM) of DLK1 is essential for LC3 accumulation on the *trans*-Golgi network, although it does not affect subcellular localization of DLK1.

DLK1 expression induces Golgi-LC3 lipidation via ATG12-ATG5-ATG16L1 complex

LC3 lipidation on the membrane compartments in autophagy and CASM is regulated by ATG multiprotein complexes (Durgan & Florey, 2022). To investigate which ATG protein complex regulates

the DLK1-induced LC3 accumulation, I observed it in HeLa cells lacking FIP200 or ATG16L1, Ulk1/2 knockout mouse embryo fibroblasts (MEFs) and Atg5 knockout MEFs. Loss of Ulk1/2 and FIP200 did not much inhibit the DLK1-induced LC3B accumulation on the *trans*-Golgi network (Figure 7. A-C). On the other hand, loss of Atg5 or ATG16L1, which are all required for ATG8 conjugation to phospholipids, completely inhibited the DLK1-induced LC3B accumulation (Figure 7. A-C). To further confirm whether LC3 is conjugated to phospholipid, LC3B G120A mutant, which replaces glycine 120 to alanine and is resistant to the cleavage by ATG4 and thus for the conjugation to phospholipids (Tanida et al, 2004), was employed. Compared to WT LC3B, LC3B G120A mutant was neither accumulated on the Golgi apparatus nor lipidated by DLK1 overexpression (Figure 8. A, B). Thus, the DLK1-induced Golgi-LC3 accumulation requires phospholipid conjugation via ATG12-ATG5-ATG16L1 complex, but not ULK1 complex, providing a new model system of Golgi-specific LC3 lipidation.

Inhibition of post-Golgi trafficking precedes Golgi-LC3 lipidation

Although several Golgi-damaging conditions were reported to induce Golgi-LC3 lipidation (Cerrato et al., 2021; Gao et al., 2016; Gomes-da-Silva et al., 2019; Liu et al., 2019), it is not clear yet whether and how LC3 lipidation is associated with different types of Golgi damage. I thus decided to systemically characterize and compare the effects of Golgi-damaging reagents on Golgi-LC3 lipidation, including the most commonly used Golgi damage inducers, brefedin A and monensin (Dinter & Berger, 1998), and the previously reported Golgi-LC3 lipidation inducers, niclosamide and AMDE-1. As reported, both niclosamide and AMDE-1 triggered robust accumulation of LC3B on the Golgi apparatus in HeLa cells (Figure 9.). In comparison with niclosamide and AMDE-1, brefeldin A caused dispersion of TGOLN2-RFP and reduced fluorescence of GFP-LC3B, and monensin induced partial recruitment of GFP-LC3B onto the Golgi apparatus. Therefore, I hypothesized that there might be a specific form of Golgi dysfunction associated with Golgi-LC3 lipidation.

Previous report, in which oleate-induced Golgi-LC3 lipidation is accompanied by protein transport inhibition at the *trans*-Golgi

network (Cerrato et al., 2021), led me to investigate whether this protein transport inhibition is a common prerequisite for Golgi-LC3 lipidation. I analyzed protein transport from the Golgi apparatus with retention using selective hooks (RUSH) system (Boncompain et al, 2012). In the RUSH system, a reporter protein fused to streptavidin-binding protein (SBP) is retained in donor compartment by a hook protein fused to streptavidin (Str) and addition of biotin releases the reporter protein by interrupting Str-SBP interaction. I utilized Str-KDEL as an endoplasmic reticulum (ER) hook protein and SBP-GFP-GPI as a reporter protein which can be released to the plasma membrane through the Golgi apparatus. As reported, biotin addition released SBP-GFP-GPI from the ER to the plasma membrane through the Golgi apparatus (Figure 10. A, B). In contrast, DLK1 overexpression blocked biotin-induced SBP-GFP-GPI transport from the *trans*-Golgi network, revealed by colocalization between SBP-GFP-GPI and Golgin-97, a *trans*-Golgi network-resident protein (Figure 10. A), clearly showing transport inhibition from the *trans*-Golgi network.

I then expanded this analysis to other Golgi-damage inducers and examined their effects on post-Golgi protein transport. As previously shown, brefeldin A and monensin prevented SBP-GFP-

GPI secretion from the ER and the Golgi apparatus, respectively (Figure 10. B). Consistent with my hypothesis, both niclosamide and AMDE-1 also blocked SBP-GFP-GPI transport from the *trans*-Golgi network (Figure 10. B). Some difference in the pattern of the Golg-LC3 lipidation among monensin, niclosamide and AMDE-1 might be due to the ionophore function of monensin in other membrane compartments as well as the Golgi apparatus (Grinde, 1983). I further determined whether LC3 lipidation itself prevents post-Golgi trafficking in HeLa cells. Post-Golgi trafficking of SBP-GFP-GPI was also inhibited by niclosamide in HeLa ATG16L1 knockout cells as well as WT cells (Figure 11.), revealing that LC3 lipidation occurs after the trafficking inhibition at the Golgi apparatus. Collectively, these data suggest that post-Golgi trafficking inhibition could be the common cause of Golgi-LC3 lipidation.

The V-ATPase-ATG16L1 axis is essential for Golgi-LC3 lipidation

V-ATPase inhibitors have previously shown to inhibit Golgi-LC3 lipidation (Gao et al., 2016; Gomes-da-Silva et al., 2019; Liu et al., 2019). I thus examined whether DLK1-induced Golgi-LC3

lipidation could also be reversed by V-ATPase inhibitors. Both V-ATPase inhibitors, Baf.A1 and ConA, abrogated the DLK1-induced LC3B accumulation and LC3B-II conversion in HeLa cells (Figure 12. A, B). By contrast, chloroquine (CQ), a lysosomotropic agents which inhibit lysosomal acidification through protonation independently of V-ATPase (Homewood et al, 1972), did not affect it (Figure 13. A, B). I also found that DLK1 overexpression promoted ATG16L1 recruitment to the *trans*-Golgi network and this recruitment was inhibited by Baf.A1 in HeLa cells (Figure 14.).

Next, to understand the mechanism of V-ATPase inhibitor-specific inhibition of Golgi-LC3 lipidation, I tested an interaction between ATG16L1 and ATP6V1A, one of the V1 subunits, in HEK293T cells exposed to niclosamide and AMDE-1, or overexpressing DLK1 (Figure 15. A, B). Immunoprecipitation assay revealed that FLAG-ATG16L1 bound to endogenous ATP6V1A. Interestingly, both niclosamide and AMDE-1 significantly increased the ATG16L1-ATP6V1A interaction, while Baf.A1 reduced this interaction (Figure 15. A). Similarly, the ATG16L1-ATP6V1A interaction was increased by DLK1 overexpression and decreased by Baf.A1 (Figure 15. B).

ATG16L1 distinguishes LC3 lipidation compartments through its WIPI2b and FIP200-binding domain (FBD) and WD40 domain (Fletcher et al, 2018; Fujita et al, 2008). To determine which domain of ATG16L1 is required for its recruitment onto the Golgi apparatus, ATG16L1 deletion mutants (Δ) were constructed. Immunoprecipitation assay in HEK293T cells showed that deletion of WD40 domain, but not FBD, completely impaired the ATG16L1-ATP6V1A interaction upon niclosamide treatment and DLK1 overexpression (Figure 16. A, B). Further, I examined the recruitment of ATG16L1 deletion mutants to the Golgi apparatus. ATG16L1 dimerizes mainly via coiled-coil domain (CCD) (Gammoh, 2020). Concerning dimerization between exogenously expressed ATG16L1 constructs and endogenous ATG16L1, I expressed different ATG16L1 constructs in HeLa ATG16L1 KO cells. Loss of ATG5-binding domain and WIPI2b/FIP200-binding domain did not affect the recruitment of ATG16L1 to the Golgi apparatus by DLK1 (Figure 17.). In contrast, loss of WD40 domain abolished colocalization between ATG16L1 and TGOLN2. Unexpectedly, I found that coiled-coil domain deletion also completely abolished ATG16L1 localization to the Golgi apparatus, suggesting that dimerization via coiled-coil domain could be essential for this

localization. These results indicate that Golgi damage recruits ATG16L1 to the Golgi apparatus through WD40 domain-dependent interaction with V-ATPase for LC3 lipidation.

Post-Golgi trafficking inhibition drives V-ATPase-ATG16L1 axis independently of pH imbalances

In CASM, ion/pH imbalances in single membranes were suggested to be unifying mechanism as they increase association of V0 and V1 subunits of V-ATPase, resulting in ATG16L1 recruitment (Durgan & Florey, 2022). To examine whether Golgi-LC3 lipidation is coupled to pH imbalances in the Golgi apparatus, I generated pHluorin-based Golgi apparatus pH sensor. pHluorin2 is a GFP2 variant which displays a bimodal excitation spectrum peaks at 395 nm and 475 nm and an emission maximum at 509 nm (Mahon, 2011). Acidification decreases pHluorin2 excitation at 395 nm but increases excitation at 475 nm, leading to 395/475 nm excitation ratios decrease. I generated Golgi-pH sensor (GALT-pH2) through conjugation of pHluorin2 to 1-82 amino acids of beta-1,4-galactosyltransferase 1 (B4GALT1), a Golgi-resident membrane protein. GALT-pH2 expression locates pHluorin2 in the Golgi lumen. Golgi apparatus localization of GALT-pH2 was confirmed as

it colocalized with TGOLN2-RFP (Figure 18. A). Using GALT-pH2, I measured Golgi pH via flow cytometry under post-Golgi trafficking inhibition by DLK1 overexpression, niclosamide and AMDE-1. Overexpression of DLK1 increased GALT-pH2 405/488 nm excitation ratios, indicating Golgi pH elevation (Figure 18. B). In contrast, DLK1 isoform 2, which cannot induce Golgi-LC3 lipidation, did not affect Golgi pH. Compared to bafilomycin A1, which neutralizes Golgi pH by V-ATPase inhibition, both Golgi-damaging reagents, niclosamide and AMDE-1, did not affect Golgi pH (Figure 18. C). These results suggest that in case of Golgi-LC3 lipidation, pH imbalances do not seem to be common prerequisite for V-ATPase-ATG16L1 axis.

Golgi membranes after LC3 lipidation are not degraded through lysosomes

As LC3 lipidation facilitates lysosomal degradation of various membranes, I checked the destiny of Golgi membranes after LC3 lipidation. Inhibiton of Golgi-LC3 lipidation by V-ATPase inhibitors is thought to operate at the stage of V0-V1 subunit assembly before LC3 lipidation occurs, rather than inducing the delipidation process itself. In addition, V-ATPase inhibition blocks lysosomal

degradation. Therefore, I hypothesized that after Golgi-LC3 lipidation, LC3 would be solely delipidated and dissociated rather than being removed through lysosomes along with Golgi membranes. To monitor lysosomal degradation of Golgi membranes, I generated tandem fluorescent-tagged TGOLN2 (TGOLN2-RFP-GFP), similar to the method of analyzing autophagic flux using tandem fluorescent-tagged LC3 (Kimura et al, 2007). Since RFP-GFP is conjugated to cytosolic domain of TGOLN2, if Golgi-derived vesicles are enclosed and degraded by autophagsomes/lysosomes, only GFP fluorescence would disappear. I first observed the fate of TGOLN2-RFP-GFP under niclosamide incubation and after the reagent was removed (Figure 19. A). Niclosamide decreased RFP-only TGOLN2 dots, which seem to be derived from post-Golgi trafficking inhibition. Even after the removal of niclosamide, the number of RFP-only dots were not increased compared to the vehicle condition. Protein levels of endogenous *trans*-Golgi network proteins, TGOLN2 and Golgin-97, were also examined by immunoblotting. TGOLN2 and Golgin-97 protein levels were not affected by incubation of niclosamide/AMDE-1 and removal of both reagents (Figure 19. B, C). TGOLN2 protein increase by chloroquine (16 h) is likely due to the inhibition of TGOLN2

turnover in basal conditions rather than effect of niclosamide and AMDE-1. In conclusion, LC3-lipidated Golgi membranes are not seem to be degraded through lysosomes.

Loss of ATG16L1 impairs TFE3 nuclear translocation in post-Golgi trafficking inhibition

I next investigated the function of LC3 lipidation during post-Golgi trafficking inhibition. I examined whether post-Golgi trafficking inhibition affects nuclear translocation of TFE3, a Golgi stress response regulator which is translocated from the cytosol to the nucleus by dephosphorylation under Golgi dysfunction (Taniguchi et al., 2015). Immunostaining of endogenous TFE3 revealed that both niclosamide and AMDE-1 treatment translocated TFE3 to the nucleus (Figure 20.). Likewise, DLK1 overexpression also induced nuclear translocation of TFE3 (Figure 21.). Then, I examined whether LC3 lipidation on the Golgi apparatus similarly affects TFE3 nuclear translocation as it activates TFEB under lysosomal damage (Nakamura et al., 2020). Unlike in WT cells, nuclear translocation of TFE3 was impaired in HeLa ATG16L1 KO cells upon niclosamide or AMDE-1 treatment (Figure 20.). The DLK1-induced nuclear translocation of TFE3 was also reduced by

ATG16L1 depletion (Figure 21.). With fractionation assay, I further confirmed that TFE3 level increased in WT nuclear fraction by those Golgi damage inducers but was impaired in ATG16L1 KO cells (Figure 22. A-D). With Phos-tag gel electrophoresis, I found that niclosamide or AMDE-1 treatment induced TFE3 dephosphorylation and these mobility shifts were reduced by ATG16L1 depletion (Figure 23.). To clarify whether autophagy, rather than LC3 lipidation itself, regulates TFE3 nuclear translocation, I examined TFE3 translocation in autophagy-deficient HeLa FIP200 KO cells. The results revealed that nuclear translocation of TFE3 was not affected in HeLa FIP200 KO cells exposed to AMDE-1 (Figure 24.).

TFE3 is involved in a wide range of cellular stress responses ranging from nutrient deprivation to various organelle damage, including ER, mitochondria and lysosome (Martina et al., 2016; Martina et al., 2014; Nezich et al., 2015; Roczniak-Ferguson et al., 2012). To address whether LC3 lipidation-mediated TFE3 regulation is specific to the Golgi stress, I examined TFE3 nuclear translocation in HeLa ATG16L1 knockout cells under several cellular stress conditions. Torin-1, tunicamycin and chloroquine were used to induce mTORC1 inhibition, ER stress, and lysosomal

damage, respectively (Figure 25.). The mTORC1 inhibition by Torin-1 translocated TFE3 to the nucleus and this translocation was not affected by loss of ATG16L1 in HeLa cells. Loss of ATG16L1 also did not affect the tunicamycin-induced TFE3 nuclear translocation. Unlike Torin-1 and tunicamycin, TFE3 nuclear translocation following lysosomal damage by chloroquine was reduced by ATG16L1 KO in HeLa cells, consistent with the function of LC3 lipidation in the lysosomal damage-induced TFEB activation (Nakamura et al., 2020). Taken together, these data suggest LC3 lipidation facilitates TFE3 activation in a Golgi stress-specific manner.

LC3 lipidation has a cytoprotective role against the Golgi damage via TFE3 activation

The Golgi stress response pathways restore Golgi homeostasis by upregulate the expression of Golgi-associated target genes (Kim et al., 2023). I thus examined the expression of TFE3 target genes as well as other Golgi stress response under Golgi damages. Consistent to TFE3 nuclear translocation, both niclosamide and AMDE-1 increased mRNA levels of TFE3 target genes (Taniguchi et al., 2015) (SIAT4A, GCP60, Giantin, WIPI49, STX3A) (Figure

26. A). Niclosamide and AMDE-1 also upregulated pro-apoptotic MCL1 isoform (MCL1-S), the target of MAPK-ETS pathway (Baumann et al., 2018). By contrast, mRNA levels of HSP47 and ARF4, the targets of HSP47 and CREB3 pathway (Miyata et al., 2013; Reiling et al., 2013), were not affected. In addition, DLK1 overexpression increased mRNA expression of TFE3 target genes as well as HSP47, ARF4 and MCL1-S (Figure 26. B). Considering the role of TFE3 in the transcription of autophagy and lysosome-related genes, I also examined expression of those genes under Golgi stress. Compared to the Golgi stress response genes, expressions of autophagy and lysosome-related genes (ATP6V1C1, MCOLN1, CTSA, ATG16L1) were not significantly increased by niclosamide and AMDE-1 except for ATP6V1C1 (Figure 26. D).

I further addressed whether LC3 lipidation facilitated upregulation of the Golgi stress response genes via TFE3. Gene expression of SIAT4A, GCP60, WIPI49, STX3A and MCL1-S which are upregulated in HeLa cells by niclosamide and AMDE-1 was compared with those in HeLa ATG16L1 KO cells. Among TFE3 target genes, WIPI49 and STX3A, vesicle transport-related genes, were not upregulated and SIAT4A and GCP60 for glycosylation and

Golgi structure, and MCL1-S were less or little affected in HeLa ATG16L1 KO cells (Figure 26. C).

As TFE3-mediated Golgi stress response has a cytoprotective role against the Golgi damage, I hypothesized that LC3 lipidation had an advantageous role in cell survival under Golgi damages. In HeLa WT cells, niclosamide and AMDE-1 treatment showed basal levels of cell toxicity less than 5%, as examined with Calcein-AM and propidium iodide (PI) staining (Figure 27. A). On the other hand, cytotoxicity induced by both chemical reagents significantly increased by the loss of ATG16L1 in HeLa cells. Upon DLK1 overexpression, cell death was not induced in HeLa WT cells, whereas it was increased 2-fold in ATG16L1-deficient cells (Figure 27. B). Together, these data suggest that LC3 lipidation on the Golgi apparatus has a cytoprotective role under Golgi damage through upregulation of the TFE3 pathway target gene expression.

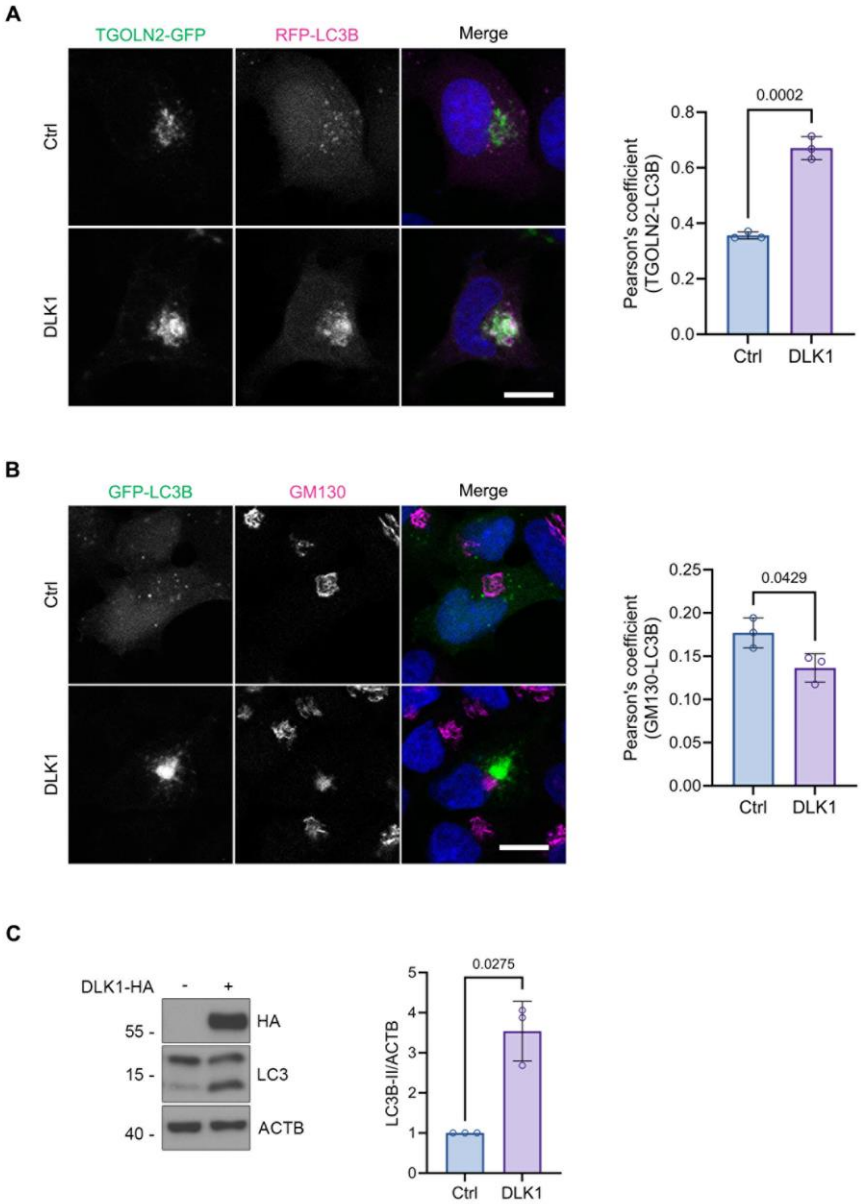
A
TGOLN2-GFP
RFP-LC3B
Merge
Ctrl
DLK1
0.0002
Pearson's coefficient (TGOLN2-LC3B)
0.8
0.6
0.4
0.2
0.0
Ctrl
DLK1
B
GFP-LC3B
GM130
Merge
Ctrl
DLK1
0.0429
Pearson's coefficient (GM130-LC3B)
0.25
0.20
0.15
0.10
0.05
0.00
Ctrl
DLK1
C
DLK1-HA
-
+
55 -
15 -
40 -
HA
LC3
ACTB
0.0275
LC3B-II/ACTB
5
4
3
2
1
0
Ctrl
DLK1

Figure 1. DLK1 overexpression accumulates LC3 on the *trans*-Golgi network.

(A, B) Confocal images of HeLa cells expressing DLK1-HA, TGOLN2-GFP and RFP-LC3B (A, left) or HeLa cells expressing DLK1-HA and GFP-LC3B and immunostained with anti-GM130 antibody (B, left). Nuclei were stained by Hoechst dye 33342. Ctrl, control. Scale bars, 10 μm. Colocalization of TGOLN2-GFP and RFP-LC3B (A, right), and of GFP-LC3B and GM130 (B, right) was quantified with Fiji and represented as Pearson's correlation coefficient. Bars represent mean ± s.d. (n = 3, 91 ~ 124 cells per experiment in A and n = 3, 51 ~ 92 cells per experiment in B, two-tailed Student's t test). (C) Immunoblot analysis of HEK293T cells expressing DLK1-HA (left). Relative signals of LC3B II to ACTB on the blots were quantified and represented as mean ± s.d. (n = 3, two-tailed Student's t test) (right).

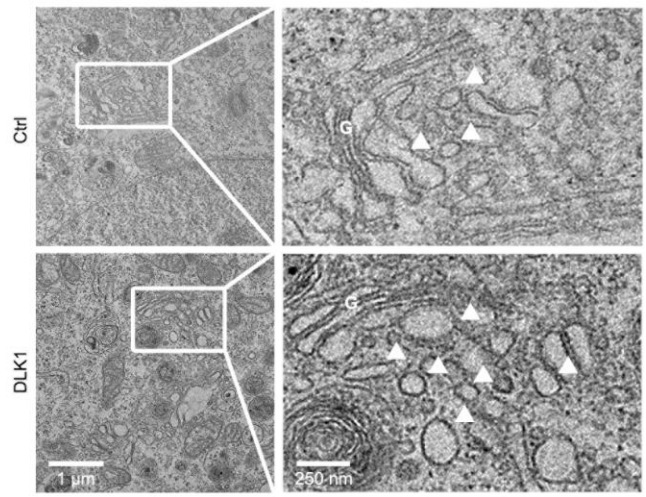
Ctrl
DLK1
G
G
1 µm
250 nm

Figure 2. DLK1 overexpression does not accumulate double-membraned autophagosomes on the *trans*-Golgi network.

Transmission electron microscopy images of HeLa cells expressing pcDNA3-HA (Ctrl) or DLK1-HA. G, Golgi apparatus. Arrow heads indicate single-membraned vesicles associated with *trans*-Golgi network.

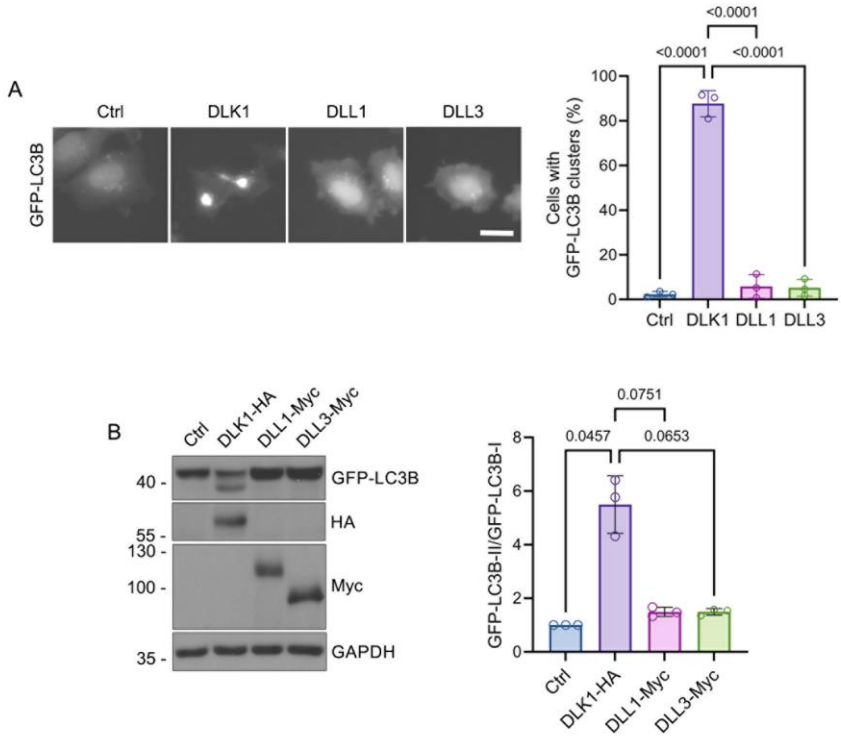
A
Ctrl
DLK1
DLL1
DLL3
GFP-LC3B
<0.0001
<0.0001
<0.0001
Cells with GFP-LC3B clusters (%)
100
80
60
40
20
0
Ctrl
DLK1
DLL1
DLL3
B
Ctrl
DLK1-HA
DLL1-Myc
DLL3-Myc
40 -
55 -
130 -
100 -
35 -
GFP-LC3B
HA
Myc
GAPDH
0.0751
0.0457
0.0653
GFP-LC3B-II/GFP-LC3B-I
8
6
4
2
0
Ctrl
DLK1-HA
DLL1-Myc
DLL3-Myc

Figure 3. DLL1 and DLL3 do not accumulate LC3 on the *trans*-Golgi network.

(A) HeLa cells expressing pcDNA3-HA (Ctrl), DLK1-HA, DLL1-Myc and DLL3-Myc together with GFP-LC3B were observed by fluoresence microscopy (left). Scale bar, 20 μm. The percentages of cells with GFP-LC3B clusters are represented as mean ± s.d. (n = 3, 71 ~ 126 cells per experiment, one-way ANOVA followed by Tukey's multiple comparisons test) (right). (B) Immunoblot analysis of HeLa cells expressing pcDNA3-HA (Ctrl), DLK1-HA, DLL1-Myc and DLL3-Myc together with GFP-LC3B (left). Relative signals if GFP-LC3B II and GFP-LC3B I on the blots are represented as mean ± s.d. (n = 3, one-way ANOVA followed by Tukey's multiple comparisons test) (right).

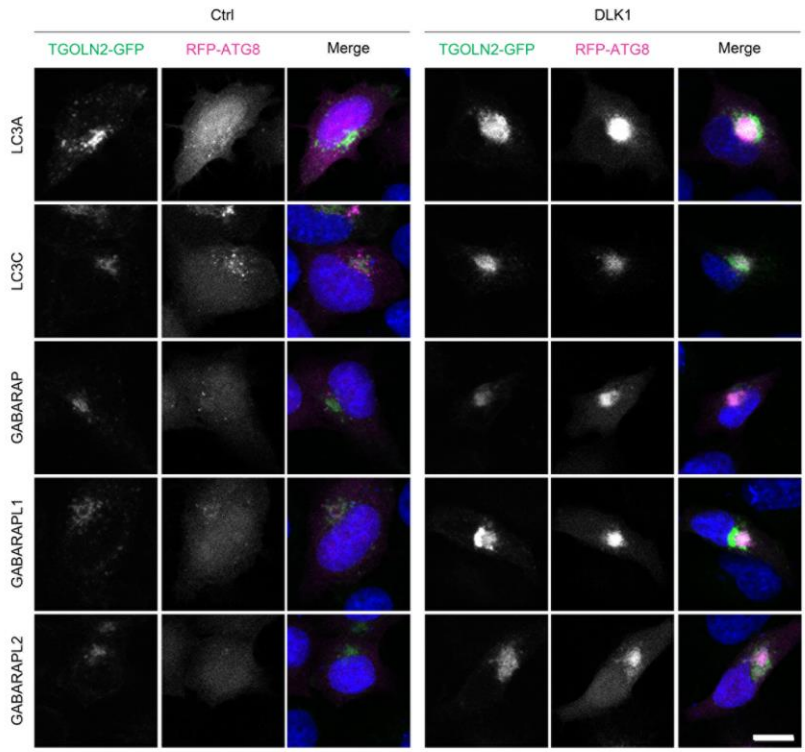
Ctrl
DLK1
TGOLN2-GFP
RFP-ATG8
Merge
TGOLN2-GFP
RFP-ATG8
Merge
LC3A
LC3C
GABARAP
GABARAPL1
GABARAPL2

Figure 4. DLK1 overexpression accumulates ATG8 family proteins on the Golgi apparatus.

Confocal images of HeLa cells expressing DLK1−HA together with TGOLN2−GFP and one of the RFP−ATG8 family proteins. Ctrl, control. Scale bar, 10 μm.

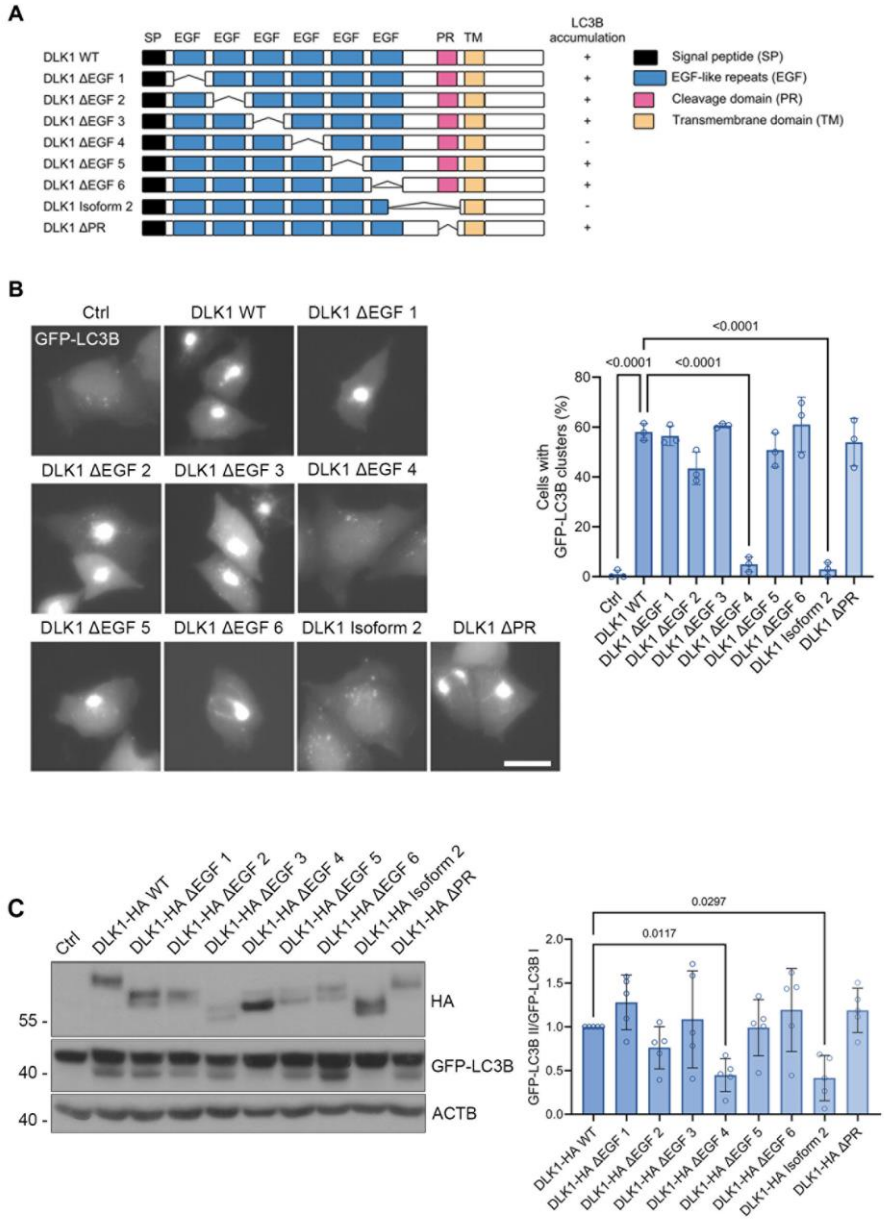
A
SP EGF EGF EGF EGF EGF EGF PR TM
LC3B accumulation
DLK1 WT +
DLK1 ΔEGF 1 +
DLK1 ΔEGF 2 +
DLK1 ΔEGF 3 +
DLK1 ΔEGF 4 -
DLK1 ΔEGF 5 +
DLK1 ΔEGF 6 +
DLK1 Isoform 2 -
DLK1 ΔPR +
Signal peptide (SP)
EGF-like repeats (EGF)
Cleavage domain (PR)
Transmembrane domain (TM)
B
Ctrl
DLK1 WT
DLK1 ΔEGF 1
GFP-LC3B
DLK1 ΔEGF 2
DLK1 ΔEGF 3
DLK1 ΔEGF 4
DLK1 ΔEGF 5
DLK1 ΔEGF 6
DLK1 Isoform 2
DLK1 ΔPR
<0.0001
<0.0001
<0.0001
Cells with GFP-LC3B clusters (%)
0
20
40
60
80
Ctrl
DLK1 WT
DLK1 ΔEGF 1
DLK1 ΔEGF 2
DLK1 ΔEGF 3
DLK1 ΔEGF 4
DLK1 ΔEGF 5
DLK1 ΔEGF 6
DLK1 Isoform 2
DLK1 ΔPR
C
Ctrl
DLK1-HA WT
DLK1-HA ΔEGF 1
DLK1-HA ΔEGF 2
DLK1-HA ΔEGF 3
DLK1-HA ΔEGF 4
DLK1-HA ΔEGF 5
DLK1-HA ΔEGF 6
DLK1-HA Isoform 2
DLK1-HA ΔPR
55 -
40 -
40 -
HA
GFP-LC3B
ACTB
0.0297
0.0117
GFP-LC3B II/GFP-LC3B I
0.0
0.5
1.0
1.5
2.0
DLK1-HA WT
DLK1-HA ΔEGF 1
DLK1-HA ΔEGF 2
DLK1-HA ΔEGF 3
DLK1-HA ΔEGF 4
DLK1-HA ΔEGF 5
DLK1-HA ΔEGF 6
DLK1-HA Isoform 2
DLK1-HA ΔPR

Figure 5. DLK1 isoform 2 does not accumulate LC3 on the *trans*-Golgi network.

(A) Schematic representation of DLK1 domains, deletion mutants and isoform. (B) HeLa cells expressing pcDNA3-HA (Ctrl), DLK1-HA WT or deletion mutants together with GFP-LC3B were observed by fluorescence microscopy (left). The percentages of cells with GFP-LC3B clusters are represented as mean ± s.d. Ctrl, control. (n = 3, 46 ~ 97 cells per experiment, one-way ANOVA followed by Tukey's multiple comparisons test) (right). Scale bar, 20 μm. (C) Immunoblot analysis of HeLa cells expressing either DLK1-HA WT or DLK1-HA mutants with GFP-LC3B (left). Relative signals of GFP-LC3B II and GFP-LC3B I on the blots are represented as mean ± s.d. Ctrl, control. (n = 5, one-way ANOVA followed by Dunnett's multiple comparisons test) (right).

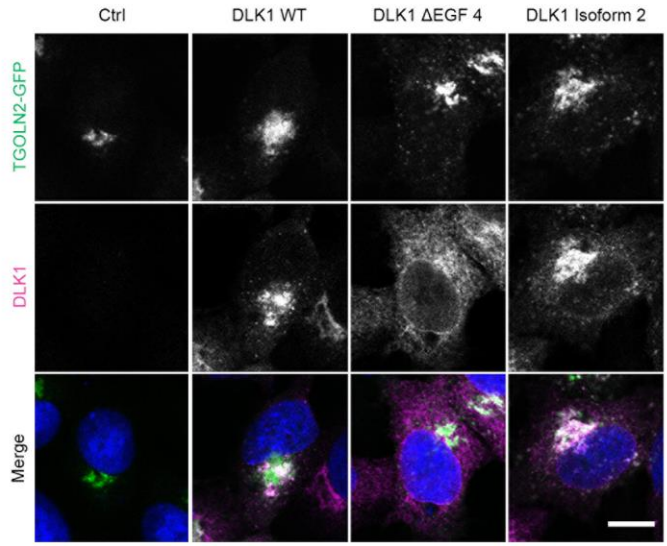
Ctrl
DLK1 WT
DLK1 ΔEGF 4
DLK1 Isoform 2
TGOLN2-GFP
DLK1
Merge

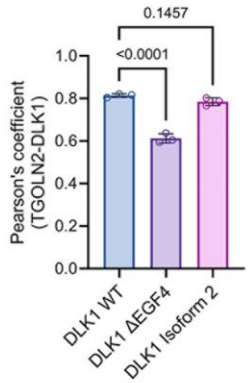
0.1457
<0.0001
1.0
0.8
0.6
0.4
0.2
0.0
Pearson's coefficient
(TGOLN2-DLK1)
DLK1 WT
DLK1 ΔEGF4
DLK1 Isoform 2

Figure 6. DLK1 WT and isoform 2 are localized in the Golgi apparatus.

Confocal microscopy images of HeLa cells expressing either DLK1-HA or DLK1-HA mutants with TGOLN2-GFP. Cells were immunostained with anti-DLK1 antibody and Nuclei were stained by Hoechst dye 33342 (top). Scale bar, 10 μm. Pearson's correlation coefficient of TGOLN2-GFP and DLK1 is represented as mean ± s.d. Ctrl, control. (n = 3, 91 ~ 125 cells per experiment, one-way ANOVA followed by Dunnett's multiple comparisons test) (bottom).

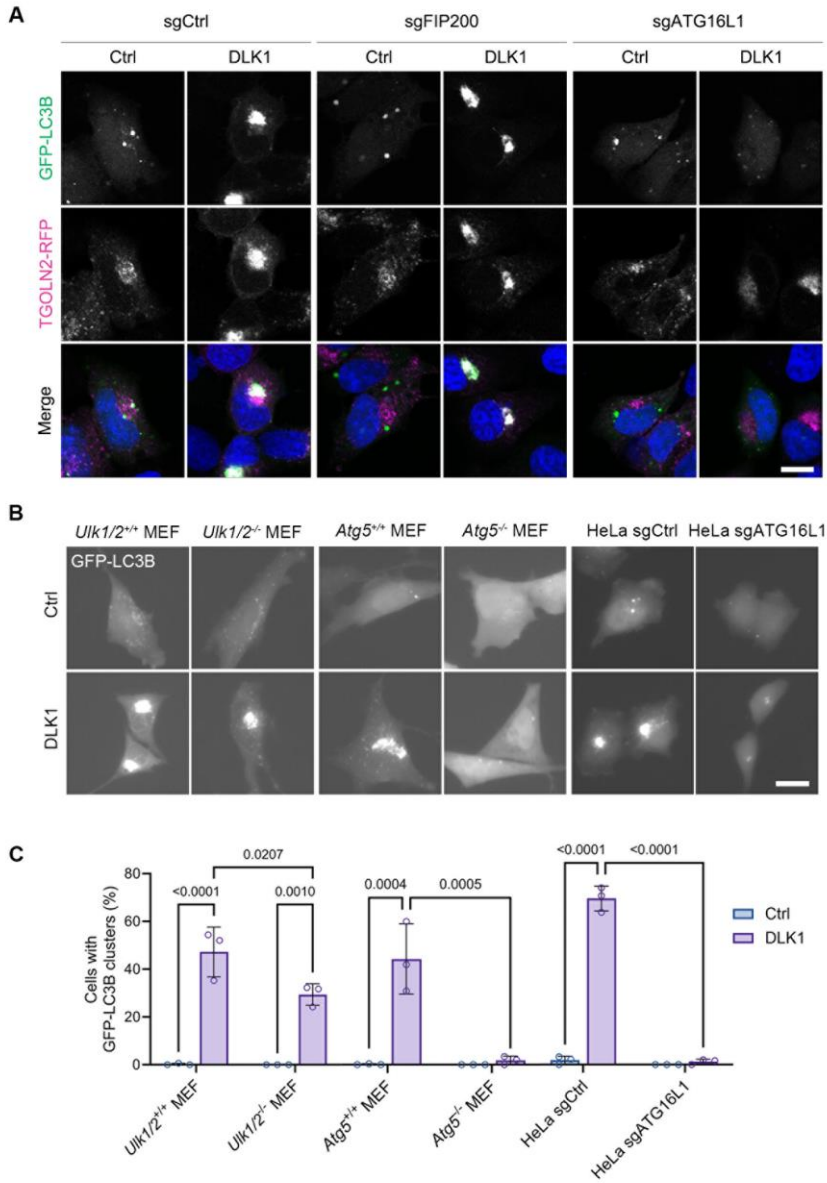
A
sgCtrl
sgFIP200
sgATG16L1
Ctrl
DLK1
Ctrl
DLK1
Ctrl
DLK1
GFP-LC3B
TGOLN2-RFP
Merge
B
Ulk1/2+/+ MEF
Ulk1/2-/- MEF
Atg5+/+ MEF
Atg5-/- MEF
HeLa sgCtrl
HeLa sgATG16L1
GFP-LC3B
Ctrl
DLK1
C
Cells with GFP-LC3B clusters (%)
0
20
40
60
80
0.0207
<0.0001
0.0010
0.0004
0.0005
<0.0001
<0.0001
Ctrl
DLK1
Ulk1/2+/+ MEF
Ulk1/2-/- MEF
Atg5+/+ MEF
Atg5-/- MEF
HeLa sgCtrl
HeLa sgATG16L1

Figure 7. LC3 accumulation on the Golgi apparatus by DLK1 expression is ATG12-ATG5-ATG16L1 complex-dependent.

(A) Confocal images of HeLa sgCtrl, sgFIP200, and sgATG16L1 cells expressing DLK1−HA, GFP−LC3B and TGOLN2−RFP. Nuclei were stained by Hoechst dye 33342. Ctrl, control. Scale bar, 10 μm. (B) Ulk1/2$^{+/+}$, Ulk1/2$^{-/-}$, Atg5$^{+/+}$, Atg5$^{-/-}$ MEFs and HeLa sgCtrl, sgATG16L1 cells expressing GFP−LC3B and either pcDNA3−HA (Ctrl) or DLK1−HA were observed by fluorescence microscopy. Scale bar, 20 μm. (C) The percentages of cells with GFP−LC3B clusters are represented as mean ± s.d. (n = 3, 84 ~ 227 cells per experiment, two−way ANOVA followed by Tukey's multiple comparisons test).

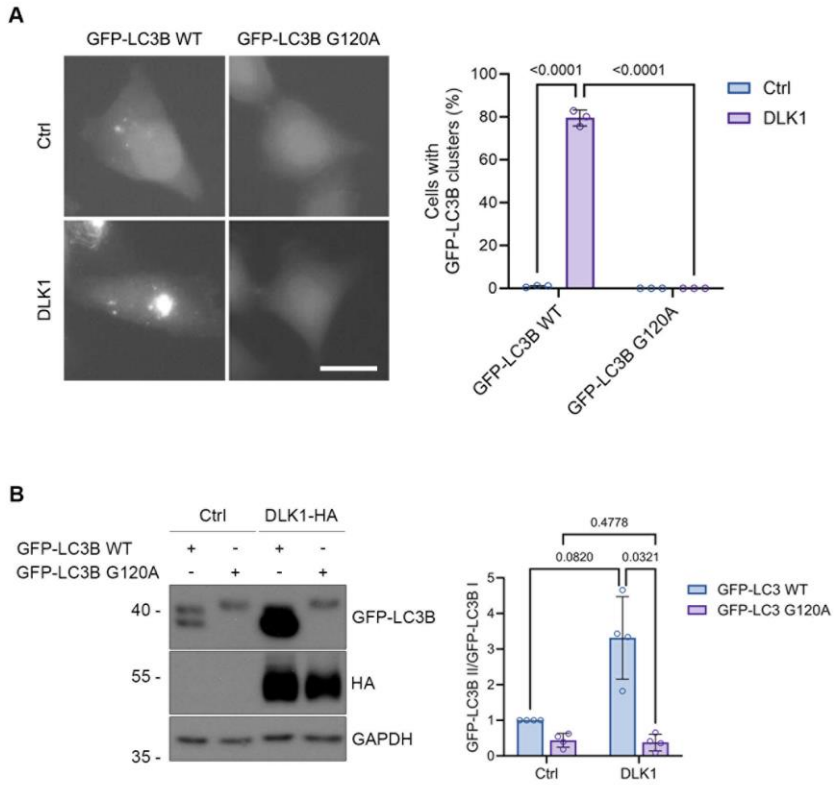
A
GFP-LC3B WT
GFP-LC3B G120A
Ctrl
DLK1
Cells with GFP-LC3B clusters (%)
<0.0001
<0.0001
Ctrl
DLK1
GFP-LC3B WT
GFP-LC3B G120A
B
Ctrl
DLK1-HA
GFP-LC3B WT
GFP-LC3B G120A
40 -
55 -
35 -
GFP-LC3B
HA
GAPDH
0.4778
0.0820
0.0321
GFP-LC3B II/GFP-LC3B I
GFP-LC3 WT
GFP-LC3 G120A
Ctrl
DLK1

Figure 8. Lipidation after C-terminal cleavage is essential for DLK1-induced LC3 accumulation on the Golgi apparatus.

(A) Fluorescence microscopy images of HeLa cells expressing DLK1-HA and either GFP-LC3B WT or GFP-LC3B G120A (left). The percentages of cells with GFP-LC3B clusters are represented as mean ± s.d. (n = 3, 115 ~ 225 cells per experiment, two-way ANOVA followed by Tukey's multiple comparisons test) (right). Scale bar, 20 μm. (B) Immunoblot analysis of HeLa cells expressing DLK1-HA WT and either GFP-LC3B WT or GFP-LC3B G120A (left). Relative signals of GFP-LC3B II and GFP-LC3B I on the blots are represented as mean ± s.d. (n = 4, two-way ANOVA followed by Tukey's multiple comparisons test) (right).

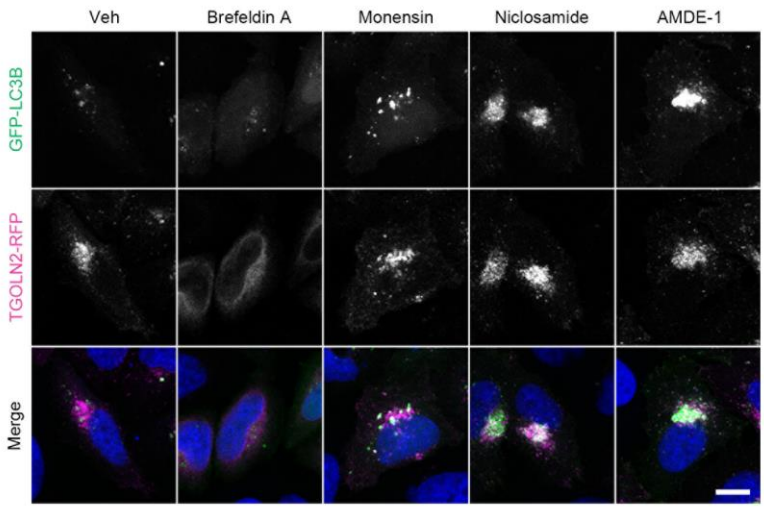
Veh
Brefeldin A
Monensin
Niclosamide
AMDE-1
GFP-LC3B
TGOLN2-RFP
Merge

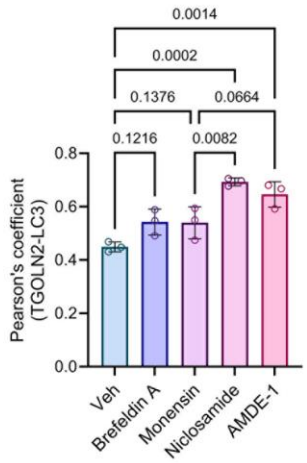
0.0014
0.0002
0.1376
0.0664
0.1216
0.0082
Pearson's coefficient (TGOLN2-LC3)
0.0
0.2
0.4
0.6
0.8
Veh
Brefeldin A
Monensin
Niclosamide
AMDE-1

Figure 9. Niclosamide and AMDE-1, but not brefeldin A and monensin, accumulate LC3 on the Golgi apparatus.

HeLa cells expressing GFP-LC3B and TGOLN2-RFP were treated with DMSO (Veh), 5 μg/ml Brefeldin A, 5 μM Monensin, 10 μM Niclosamide or 10 μM AMDE-1 for 6 h and observed by confocal microscopy. Nuclei were stained by Hoechst dye 33342 (top). Scale bar, 10 μm. Pearson's correlation coefficient of TGOLN2-GFP and RFP-LC3B is represented as mean ± s.d. (n = 3, 53 ~ 121 cells per experiment, one-way ANOVA followed by Tukey's multiple comparisons test) (bottom).

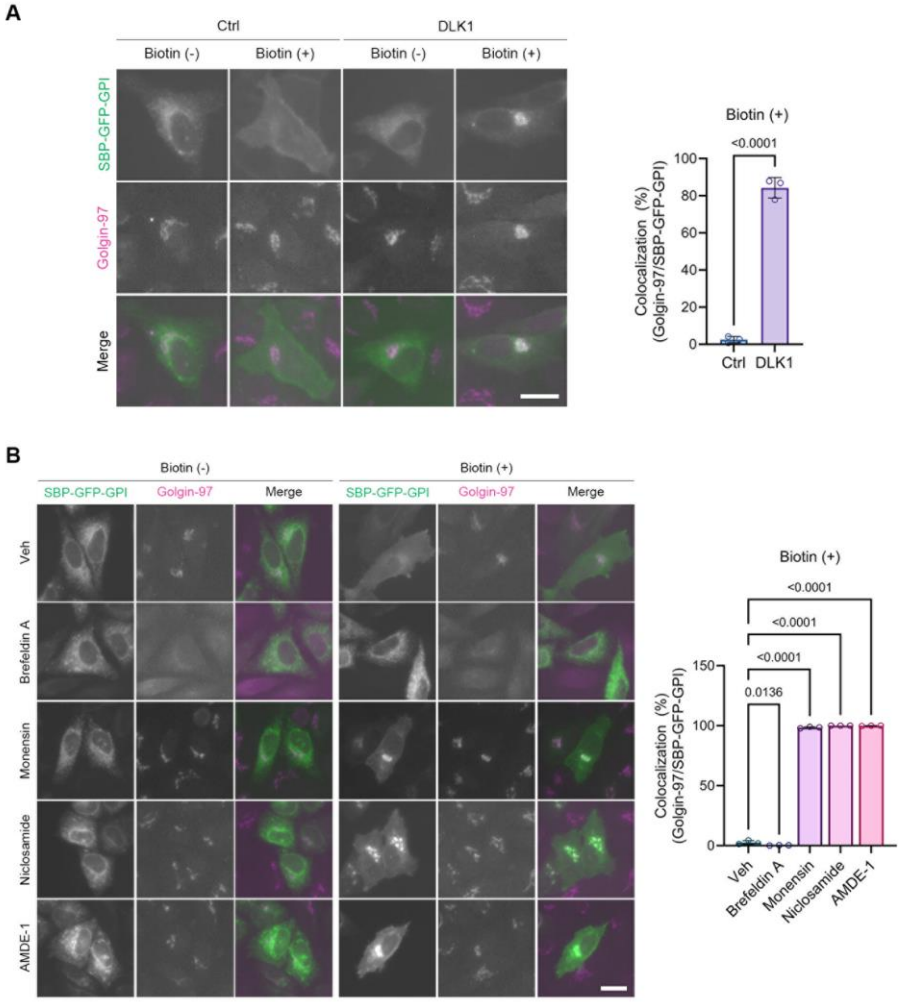
A
Ctrl
DLK1
Biotin (-)
Biotin (+)
Biotin (-)
Biotin (+)
SBP-GFP-GPI
Golgin-97
Merge
Biotin (+)
<0.0001
Colocalization (%)
(Golgin-97/SBP-GFP-GPI)
100
80
60
40
20
0
Ctrl
DLK1
B
Biotin (-)
Biotin (+)
SBP-GFP-GPI
Golgin-97
Merge
SBP-GFP-GPI
Golgin-97
Merge
Veh
Brefeldin A
Monensin
Niclosamide
AMDE-1
Biotin (+)
<0.0001
<0.0001
<0.0001
0.0136
Colocalization (%)
(Golgin-97/SBP-GFP-GPI)
150
100
50
0
Veh
Brefeldin A
Monensin
Niclosamide
AMDE-1

Figure 10. DLK1 overexpression, niclosamide and AMDE-1 inhibit post-Golgi trafficking.

(A) HeLa cells expressing STR-KDEL_SBP-GFP-GPI were treated with DMSO (Veh), 5 μg/ml Brefeldin A, 5 μM Monensin, 10 μM Niclosamide, or 10 μM AMDE-1 for 6 h and treated with 100 μM biotin for additional 2 h. Cells were immunostained with anti-Golgin-97 antibody and observed by fluorescence microscopy (left). Scale bar, 20 μm. The percentages of cells showing SBP-GFP-GPI trafficking inhibition are represented as mean ± s.d. (n = 3, 290 ~ 489 cells per experiment, one-way ANOVA followed by Dunnett's multiple comparisons test) (right). (B) HeLa cells expressing DLK1-HA and STR-KDEL_SBP-GFP-GPI were treated with 100 μM biotin, immunostained with anti-Golgin-97 antibody, and observed by fluorescence microscopy (left). Scale bar, 20 μm. Ctrl, control. The percentages of cells showing SBP-GFP-GPI trafficking inhibition are represented as mean ± s.d. (n = 3, 74 ~ 120 cells per experiment, two-tailed Student's t test) (right).

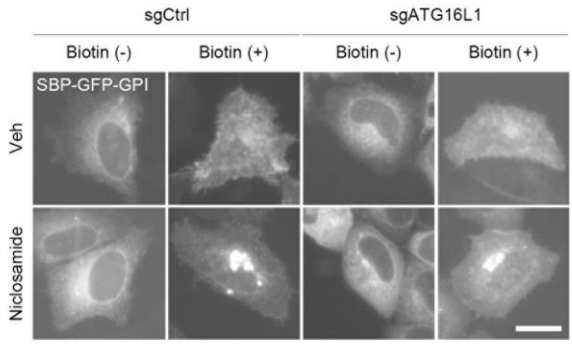
sgCtrl
sgATG16L1
Biotin (-)
Biotin (+)
Biotin (-)
Biotin (+)
SBP-GFP-GPI
Veh
Niclosamide

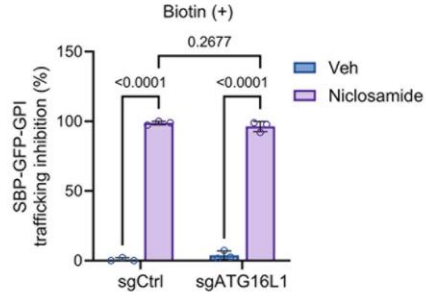
Biotin (+)
0.2677
<0.0001
<0.0001
Veh
Niclosamide
SBP-GFP-GPI trafficking inhibition (%)
150
100
50
0
sgCtrl
sgATG16L1

Figure 11. Post-Golgi trafficking inhibition precedes Golgi-LC3 lipidation.

HeLa sgCtrl, ATG16L1 cells expressing STR-KDEL_SBP-GFP-GPI were treated with 10 μM niclosamide for 6 h and then treated with 100 μM biotin for 2 h. Cells were observed by fluorescence microscopy (top). Scale bar, 20 μm. The percentages of cells showing SBP-GFP-GPI trafficking inhibition are represented as mean ± s.d. (n = 3, 75 ~ 194 cells per experiment, two-way ANOVA followed by Tukey's multiple comparisons test) (bottom).

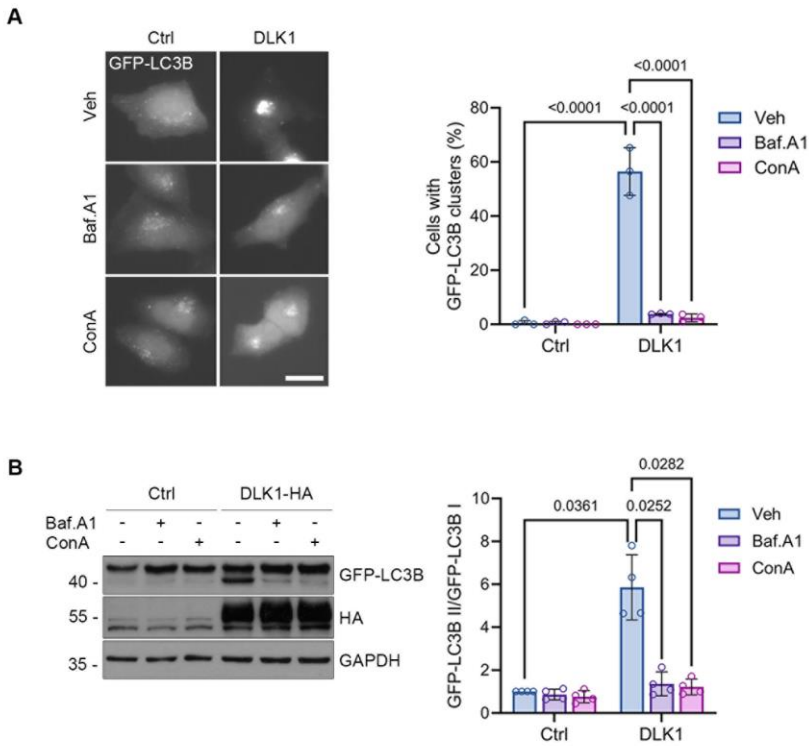
A
Ctrl
DLK1
GFP-LC3B
Veh
Baf.A1
ConA
Cells with GFP-LC3B clusters (%)
<0.0001
<0.0001
<0.0001
Veh
Baf.A1
ConA
Ctrl
DLK1
B
Ctrl
DLK1-HA
Baf.A1
ConA
40 -
55 -
35 -
GFP-LC3B
HA
GAPDH
GFP-LC3B II/GFP-LC3B I
0.0282
0.0361
0.0252
Veh
Baf.A1
ConA
Ctrl
DLK1

Figure 12. V-ATPase inhibitors reverse DLK1-induced LC3 lipidation.

(A) HeLa cells expressing DLK1-HA and GFP-LC3B were treated with 20 nM bafilomycin A1 (Baf.A1) or 200 nM concanamycin A (ConA) for 6 h and observed by fluorescence microscopy (left). Scale bar, 20 μm. The percentages of cells with GFP-LC3 clusters are represented as mean ± s.d. Ctrl, control. (n = 3, 90 ~ 199 cells per experiment, two-way ANOVA followed by Tukey's multiple comparisons test) (right). (B) HeLa cells expressing DLK1-HA and GFP-LC3B were treated with 20 nM bafilomycin A1 (Baf.A1) or 200 nM concanamycin A (ConA) for 6 h and subjected to immunoblot analysis (left). Relative signals of GFP-LC3B II and GFP-LC3B I on the blots are represented as mean ± s.d. (n = 4, two-way ANOVA followed by Tukey's multiple comparisons test) (right).

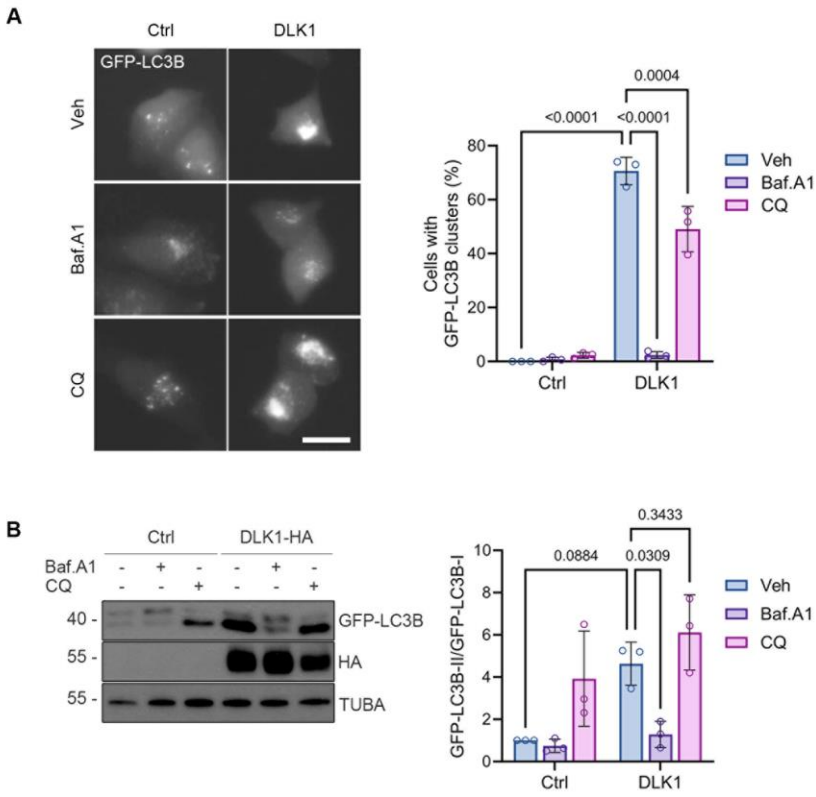
A
Ctrl
DLK1
GFP-LC3B
Veh
Baf.A1
CQ
Cells with GFP-LC3B clusters (%)
<0.0001
<0.0001
0.0004
Veh
Baf.A1
CQ
Ctrl
DLK1
B
Ctrl
DLK1-HA
Baf.A1
CQ
40 -
55 -
55 -
GFP-LC3B
HA
TUBA
GFP-LC3B-II/GFP-LC3B-I
0.0884
0.0309
0.3433
Veh
Baf.A1
CQ
Ctrl
DLK1

Figure 13. Chloroquine does not inhibit DLK1-induced LC3 lipidation.

(A) HeLa cells expressing DLK1-HA and GFP-LC3B were treated with 20 nM bafilomycin A1 (Baf.A1) or 100 μM chloroquine (CQ) for 6 h and observed by fluorescence microscopy (left). Scale bar, 20 μm. The percentages of cells with GFP-LC3B clusters are represented as mean ± s.d. (n = 3, 139 ~ 240 cells per experiment, two-way ANOVA followed by Tukey's multiple comparisons test) (right). (B) HeLa cells expressing DLK1-HA and GFP-LC3B were treated with 20 nM bafilomycin A1 (Baf.A1) or 100 μM chloroquine (CQ) for 6 h and subjected to immunoblot analysis (left). Relative signals of GFP-LC3B II and GFP-LC3B I on the blots are represented as mean ± s.d. (n = 3, two-way ANOVA followed by Tukey's multiple comparisons test) (right).

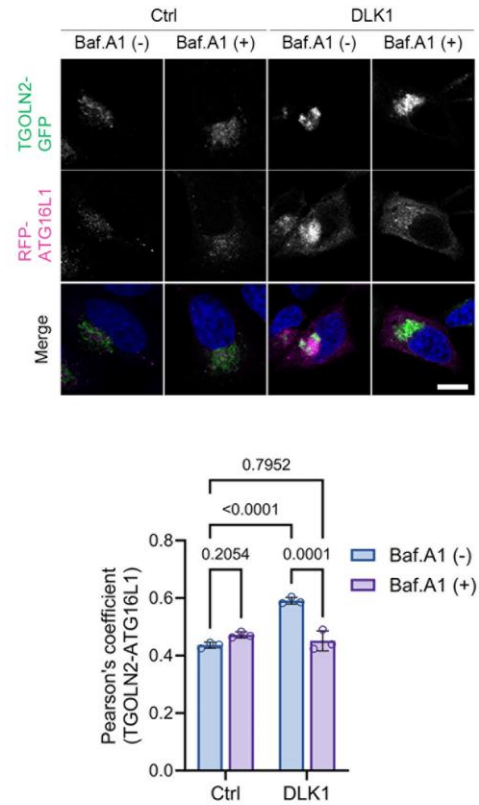
Ctrl
DLK1
Baf.A1 (-)
Baf.A1 (+)
Baf.A1 (-)
Baf.A1 (+)
TGOLN2-GFP
RFP-ATG16L1
Merge
0.7952
<0.0001
0.2054
0.0001
Baf.A1 (-)
Baf.A1 (+)
Pearson's coefficient (TGOLN2-ATG16L1)
0.8
0.6
0.4
0.2
0.0
Ctrl
DLK1

Figure 14. DLK1 overexpression recruits ATG16L1 to the Golgi apparatus via V-ATPase-dependent manner.

HeLa cells expressing DLK1-HA, TGOLN2-GFP and RFP-ATG16L1 were treated with 20 nM bafilomycin A1 (Baf.A1) for 6 h and observed by confocal microscopy. Nuclei were stained by Hoechst dye 33342. Ctrl, control (top). Scale bar, 10 μm. Pearson's correlation coefficient of TGOLN2-GFP and RFP-ATG16L1 is represented as mean ± s.d. (n = 3, 63 ~ 123 cells per experiment, two-way ANOVA followed by Tukey's multiple comparisons test) (bottom).

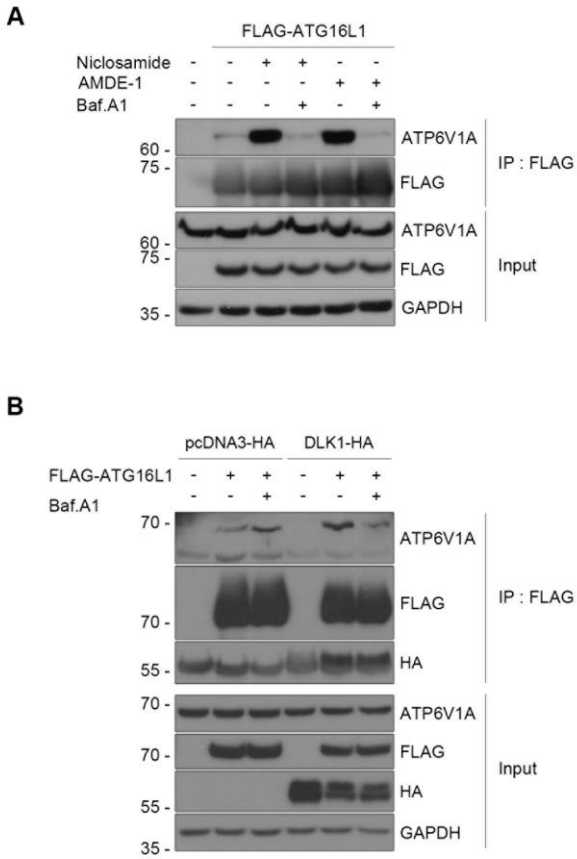
A
FLAG-ATG16L1
Niclosamide - - + + - -
AMDE-1 - - - - + +
Baf.A1 - - - + - +
60 -
75 -
ATP6V1A
FLAG
IP : FLAG
60 -
75 -
ATP6V1A
FLAG
Input
35 -
GAPDH
B
pcDNA3-HA
DLK1-HA
FLAG-ATG16L1 - + + - + +
Baf.A1 - - + - - +
70 -
ATP6V1A
FLAG
IP : FLAG
70 -
55 -
HA
70 -
ATP6V1A
70 -
FLAG
Input
55 -
HA
35 -
GAPDH

Figure 15. Golgi stress-induced ATG16L1-ATP6V1A interaction is inhibited by V-ATPase inhibitor.

(A) HEK293T cells expressing FLAG-ATG16L1 were incubated with 10 μM niclosamide or 10 μM AMDE-1 for 4 h and treated with 20 nM bafilomycin A1 (Baf.A1) for additional 3 h. Cells were subjected to immunoprecipitation (IP) assay with anti-FLAG M2 Affinity Gel. Immunoprecipitates and whole cell lysates (Input) were analyzed by immunoblotting. (B) HEK293T cells expressing DLK1-HA with or without FLAG-ATG16L1 were treated with 20 nM bafilomycin A1 (Baf.A1) for 6 h and subjected to immunoprecipitation (IP) assay with anti-FLAG M2 Affinity Gel.

A

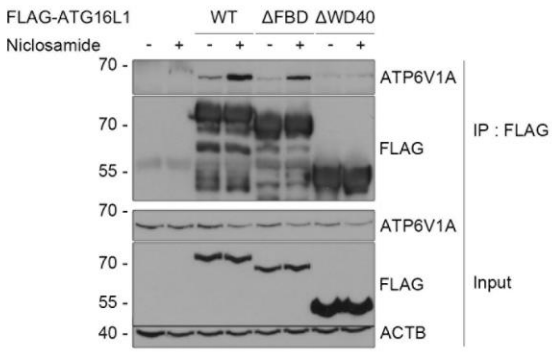
FLAG-ATG16L1
WT
ΔFBD
ΔWD40
Niclosamide
- + - + - + - +
70 -
ATP6V1A
70 -
55 -
FLAG
IP : FLAG
70 -
ATP6V1A
70 -
55 -
FLAG
Input
40 -
ACTB

B

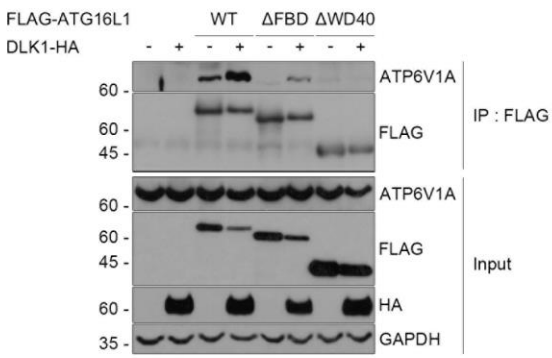
FLAG-ATG16L1
WT
ΔFBD
ΔWD40
DLK1-HA
- + - + - + - +
60 -
ATP6V1A
60 -
45 -
FLAG
IP : FLAG
60 -
ATP6V1A
60 -
45 -
FLAG
Input
60 -
HA
35 -
GAPDH

Figure 16. WD40 domain of ATG16L1 is required for ATG16L1-ATP6V1A interaction under Golgi stress.

(A) HEK293T cells expressing FLAG-ATG16L1 WT or FLAG-ATG16L1 mutants were incubated with 10 μM niclosamide for 6 h and subjected to immunoprecipitation (IP) assay with anti-FLAG M2 Affinity Gel. (B) HEK293T cells expressing DLK1-HA with FLAG-ATG16L1 WT or FLAG-ATG16L1 mutants were subjected to immunoprecipitation (IP) assay with anti-FLAG M2 Affinity Gel.

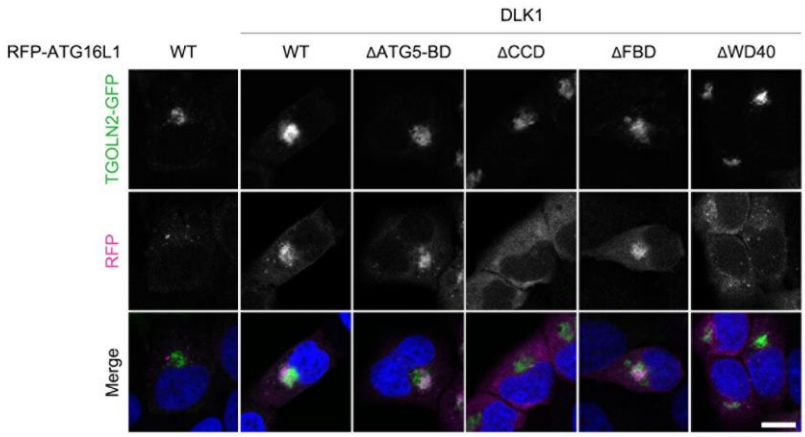
DLK1
RFP-ATG16L1
WT
WT
ΔATG5-BD
ΔCCD
ΔFBD
ΔWD40
TGOLN2-GFP
RFP
Merge

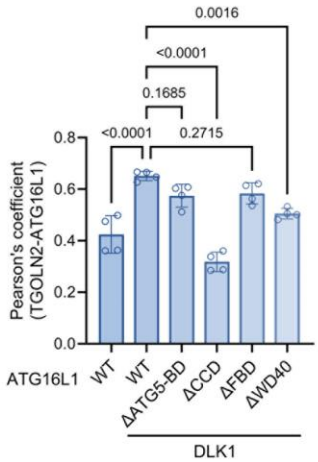
0.0016
<0.0001
0.1685
<0.0001
0.2715
Pearson's coefficient
(TGOLN2-ATG16L1)
0.8
0.6
0.4
0.2
0.0
ATG16L1
WT
WT
ΔATG5-BD
ΔCCD
ΔFBD
ΔWD40
DLK1

Figure 17. WD40 and coiled-coil domain of ATG16L1 are required for DLK1-induced ATG16L1 recruitment to the Golgi apparatus.

Confocal images of HeLa cells expressing DLK1-HA, TGOLN2-GFP and RFP-ATG16L1 mutants. Nuclei were stained by Hoechst dye 33342 (top). Scale bar, 10 μm. Pearson's correlation coefficient of TGOLN2-GFP and RFP-ATG16L1 is represented as mean ± s.d. (n = 4, 21 ~ 67 cells per experiment, one-way ANOVA followed by Tukey's multiple comparisons test) (bottom).

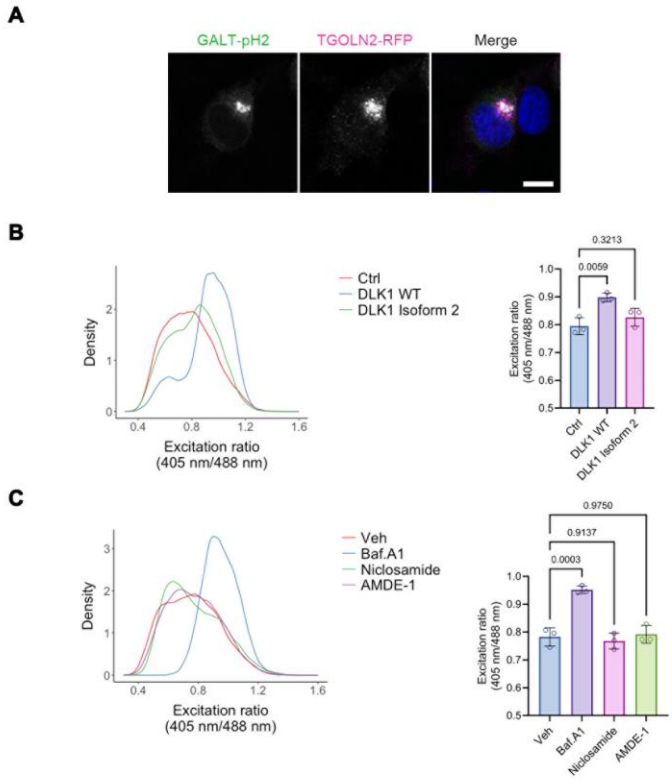
A
GALT-pH2
TGOLN2-RFP
Merge
B
Density
Excitation ratio
(405 nm/488 nm)
Ctrl
DLK1 WT
DLK1 Isoform 2
0.3213
0.0059
Excitation ratio
(405 nm/488 nm)
Ctrl
DLK1 WT
DLK1 Isoform 2
C
Density
Excitation ratio
(405 nm/488 nm)
Veh
Baf.A1
Niclosamide
AMDE-1
0.9750
0.9137
0.0003
Excitation ratio
(405 nm/488 nm)
Veh
Baf.A1
Niclosamide
AMDE-1

Figure 18. DLK1 overexpression, but not niclosamide and AMDE-1, induces Golgi-pH imbalances.

(A) Confocal images of HeLa cells expressing GALT-pH2 and TGOLN2-RFP. Nuclei were stained by Hoechst dye 33342. Scale bar, 10 μm. (B) HeLa cells expressing pcDNA3-HA (Ctrl), DLK1-HA WT or DLK1 Isoform 2 together with GALT-pH2 were subjected to flow cytometry. Frequency distributions of excitation ratios (405/408 nm) are shown (left). Median values of excitation ratios (405/408 nm) are represented as mean ± s.d. (n = 3, one-way ANOVA followed by Tukey's multiple comparisons test) (right). (C) HeLa cells expressing GALT-pH2 were treated with 20 nM bafilomycin A1 (Baf.A1), 10 μM niclosamide or 10 μM AMDE-1 for 6 h and subjected to flow cytometry. Frequency distributions of excitation ratios (405/408 nm) are shown (left). Median values of excitation ratios (405/408 nm) are represented as mean ± s.d. (n = 3, one-way ANOVA followed by Tukey's multiple comparisons test) (right).

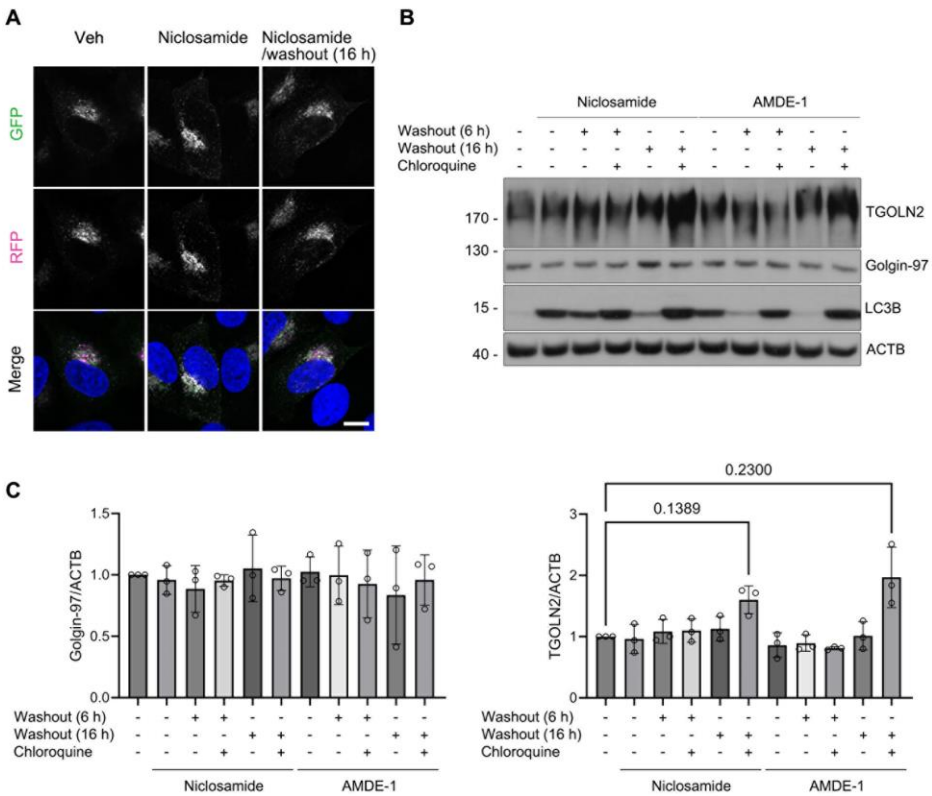
A
Veh
Niclosamide
Niclosamide /washout (16 h)
GFP
RFP
Merge
B
Niclosamide
AMDE-1
Washout (6 h)
Washout (16 h)
Chloroquine
170 -
130 -
15 -
40 -
TGOLN2
Golgin-97
LC3B
ACTB
C
Golgin-97/ACTB
1.5
1.0
0.5
0.0
Washout (6 h)
Washout (16 h)
Chloroquine
Niclosamide
AMDE-1
0.2300
0.1389
TGOLN2/ACTB
3
2
1
0

Figure 19. LC3-lipidated Golgi membranes are not degraded via lysosomes.

(A) HeLa cells expressing TGOLN2-RFP-GFP were incubated with 10 μM niclosamide for 6 h and niclosamide was removed for additional 16 h. Nuclei were stained by Hoechst dye 33342. Scale bar, 10 μm. (B) HeLa cells were incubated with 10 μM niclosamide or 10 μM AMDE-1 for 6 h. Niclosamide and AMDE-1 were removed for additional 6 h or 16 h in the presence or absence of 50 μM chloroquine. Cells were subjected to immunoblot analysis. (C) Relative signals of Golgin-97 and ACTB (left), TGOLN2 and ACTB (right) on the blots of (B) are represented as mean ± s.d. (n = 3, one-way ANOVA followed by Tukey's multiple comparisons test). are represented as mean ± s.d. (n = 3, one-way ANOVA followed by Tukey's multiple comparisons test) (right).

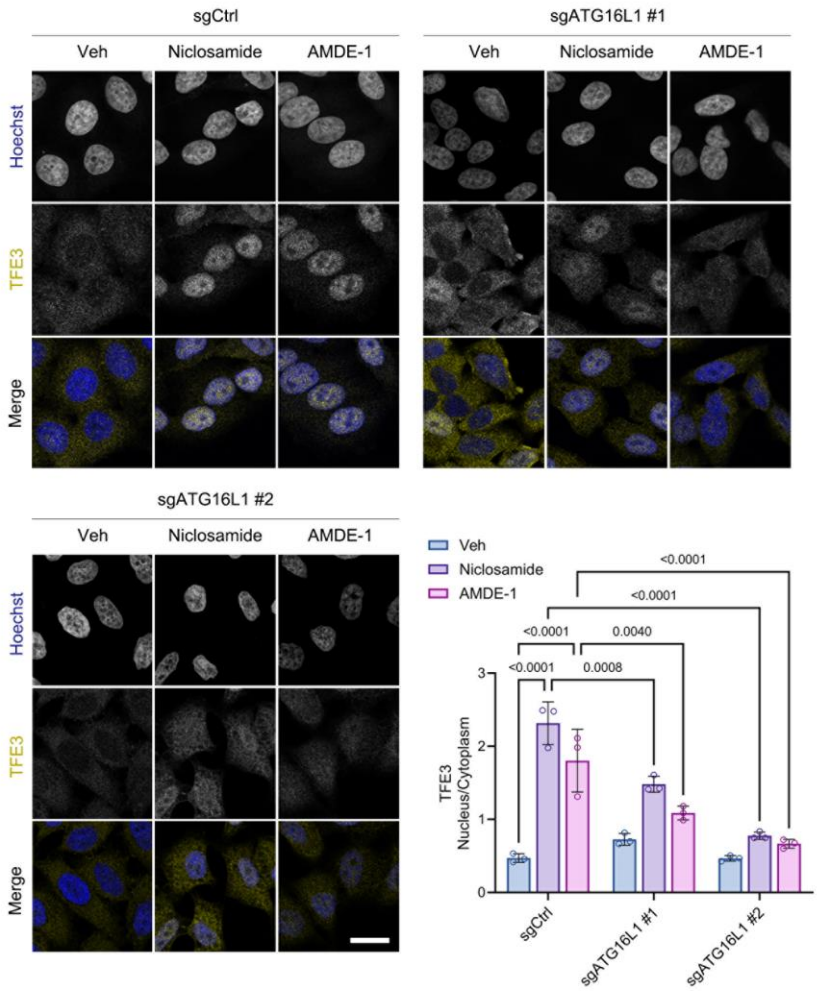
sgCtrl
sgATG16L1 #1
sgATG16L1 #2
Veh
Niclosamide
AMDE-1
Hoechst
TFE3
Merge
Veh
Niclosamide
AMDE-1
<0.0001
<0.0001
<0.0001
0.0040
<0.0001
0.0008
TFE3
Nucleus/Cytoplasm
0
1
2
3
sgCtrl
sgATG16L1 #1
sgATG16L1 #2

Figure 20. ATG16L1 knockout impairs TFE3 nuclear translocation under niclosamide and AMDE-1 treatment.

Confocal images of HeLa sgCtrl, sgATG16L1 #1, and sgATG16L1 #2 cells incubated with 10 μM niclosamide or 10 μM AMDE−1 for 6 h and immunostained with anti−TFE3 antibody. Nuclei were stained by Hoechst dye 33342. Scale bar, 10 μm. The nucleus/cytoplasm ratio of TFE3 fluorescence intensity is represented as mean ± s.d. (n = 3, 107 ~ 224 cells per experiment, two−way ANOVA followed by Tukey's multiple comparisons test) (botton, right).

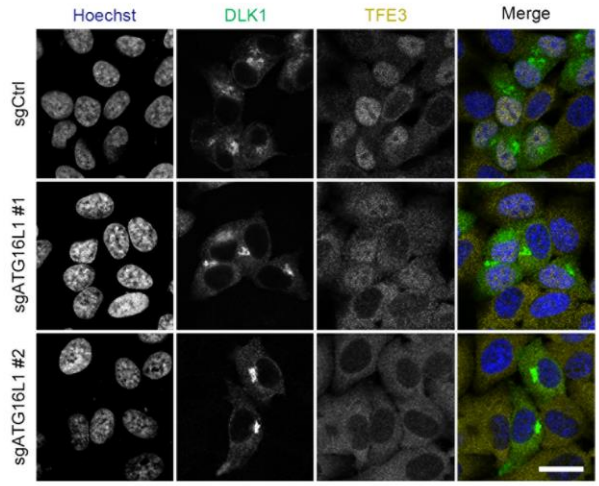
Hoechst
DLK1
TFE3
Merge
sgCtrl
sgATG16L1 #1
sgATG16L1 #2

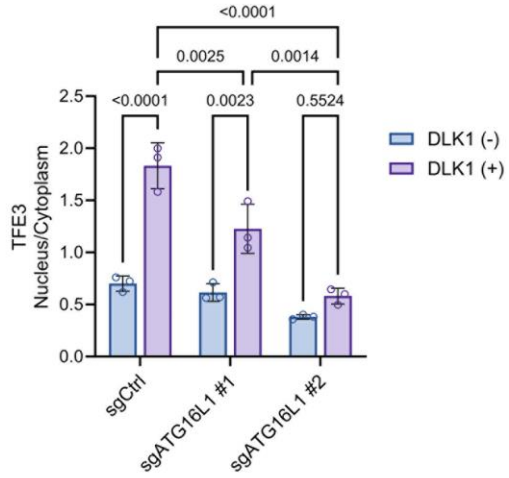
<0.0001
0.0025
0.0014
<0.0001
0.0023
0.5524
TFE3
Nucleus/Cytoplasm
2.5
2.0
1.5
1.0
0.5
0.0
DLK1 (-)
DLK1 (+)
sgCtrl
sgATG16L1 #1
sgATG16L1 #2

Figure 21. ATG16L1 knockout impairs TFE3 nuclear translocation under DLK1 overexpression.

Confocal images of HeLa sgCtrl, sgATG16L1 #1, and sgATG16L1 #2 cells expressing DLK1−HA and immunostained with anti−DLK1 and anti−TFE3 antibody. Nuclei were stained by Hoechst dye 33342 (top). Scale bar, 10 μm. The nucleus/cytoplasm ratio of TFE3 fluorescence intensity is represented as mean ± s.d. (n = 3, 46 ~ 247 cells per experiment, two−way ANOVA followed by Tukey's multiple comparisons test) (bottom).

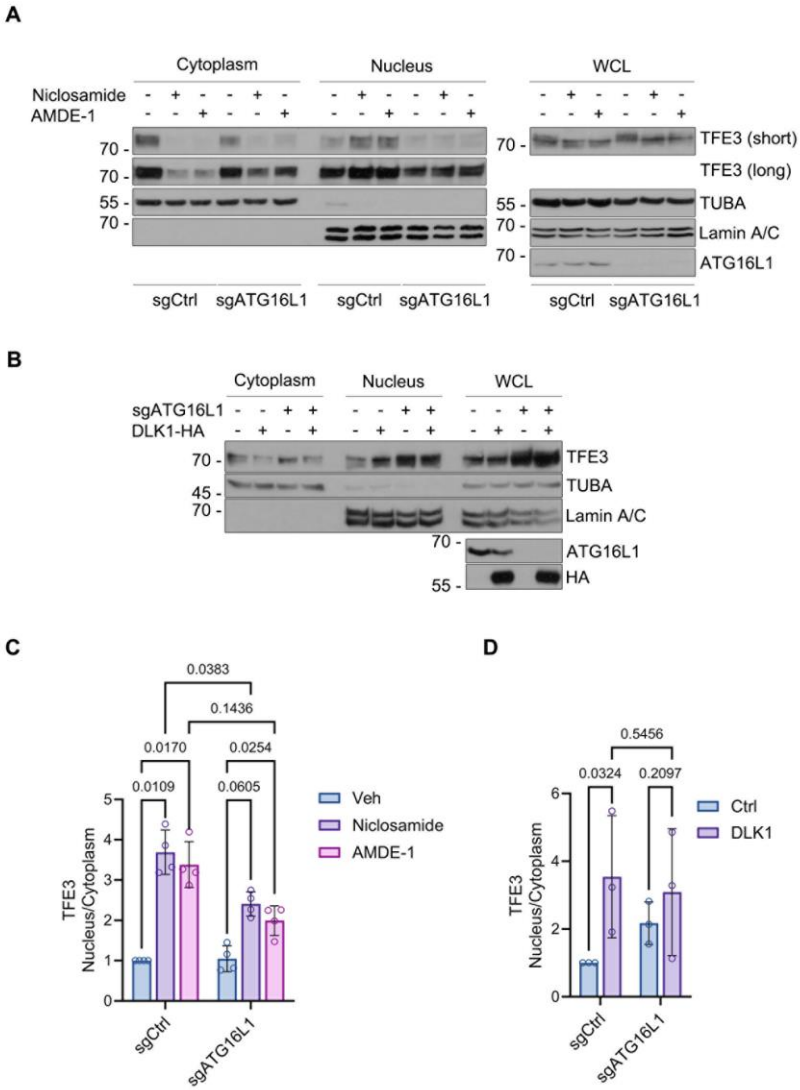
A
Cytoplasm
Nucleus
WCL
Niclosamide
AMDE-1
70 -
70 -
55 -
70 -
TFE3 (short)
TFE3 (long)
TUBA
Lamin A/C
ATG16L1
sgCtrl
sgATG16L1
B
sgATG16L1
DLK1-HA
45 -
TFE3
HA
C
0.0383
0.1436
0.0170
0.0254
0.0109
0.0605
Veh
Niclosamide
AMDE-1
TFE3 Nucleus/Cytoplasm
D
0.5456
0.0324
0.2097
Ctrl
DLK1

Figure 22. ATG16L1 knockout impairs TFE3 nuclear translocation in post-Golgi trafficking inhibition.

(A, B) Immunoblot analysis of nuclear and cytoplasmic fractions, and whole cell lysates (WCL) of HeLa sgCtrl and sgATG16L1 cells after incubation with 10 μM niclosamide or 10 μM AMDE−1 for 6 h (A) or expressing pcDNA3−HA (Ctrl) or DLK1−HA (B). (C, D) Relative signal intensities of nuclear and cytoplasmic TFE3 in A (C) and B (D) are represented as mean ± s.d. [n = 4 (C), n = 3 (D), two−way ANOVA followed by Tukey's multiple comparisons test)].

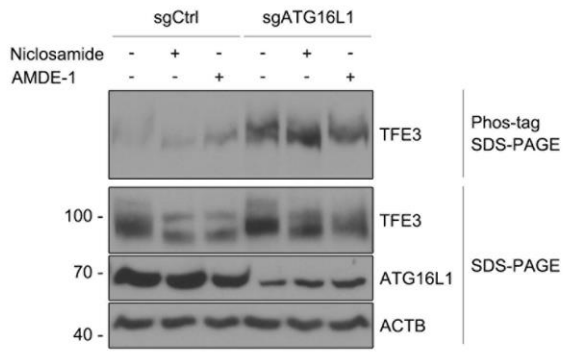
sgCtrl
sgATG16L1
Niclosamide - + - - + -
AMDE-1 - - + - - +
TFE3
Phos-tag SDS-PAGE
100 -
TFE3
70 -
ATG16L1
SDS-PAGE
40 -
ACTB

Figure 23. ATG16L1 knockout impairs TFE3 dephosphorylation in post-Golgi trafficking inhibition.

Phos-tag SDS-PAGE analysis of TFE3 in HeLa sgCtrl and sgATG16L1 cells after incubation with 10 μM niclosamide or 10 μM AMDE-1 for 6 h.

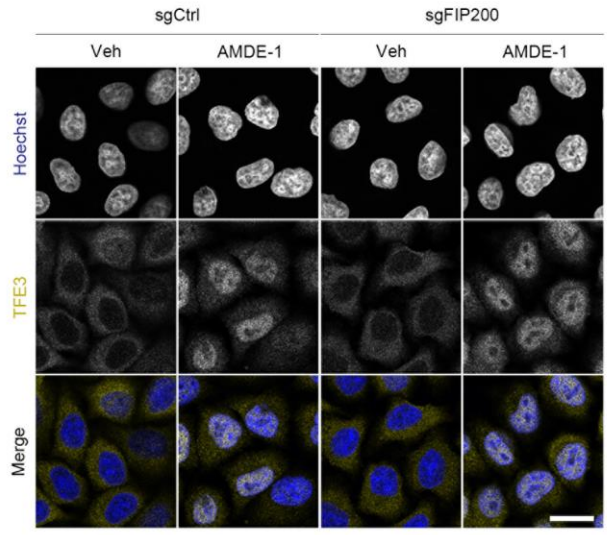
sgCtrl
sgFIP200
Veh
AMDE-1
Veh
AMDE-1
Hoechst
TFE3
Merge

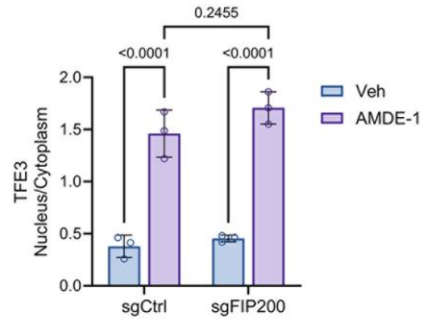
0.2455
<0.0001
<0.0001
2.0
1.5
1.0
0.5
0.0
TFE3
Nucleus/Cytoplasm
sgCtrl
sgFIP200
Veh
AMDE-1

Figure 24. FIP200-independent TFE3 regulation under Golgi-stress.

Confocal microscopy images of HeLa sgCtrl and sgFIP200 cells exposed to 10 μM AMDE−1 for 6 h and immunostained with anti−TFE3 antibody. Nuclei were stained by Hoechst dye 33342 (top). Scale bar, 10 μm. The nucleus/cytoplasm ratio of TFE3 fluorescence intensity is represented as mean ± s.d. (n = 3, 154 ~ 216 cells per experiment, two−way ANOVA followed by Tukey's multiple comparisons test) (bottom).

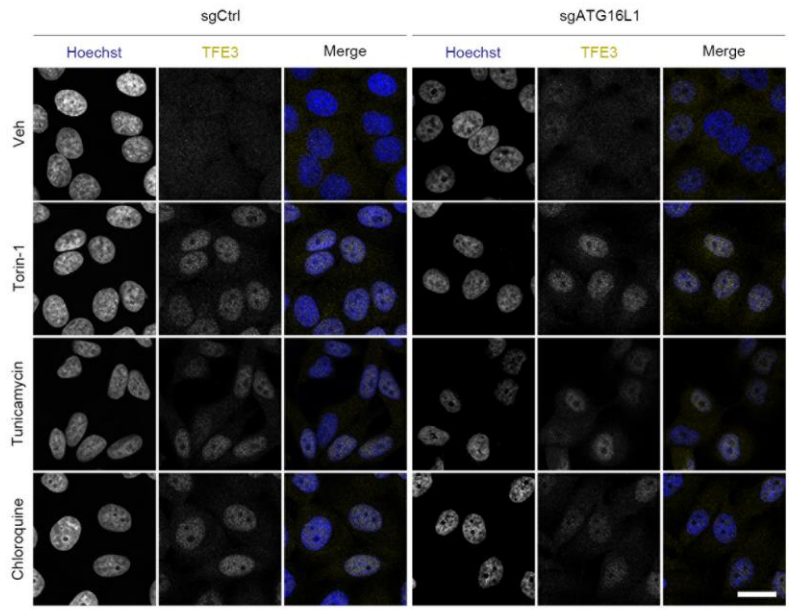
sgCtrl
sgATG16L1
Hoechst
TFE3
Merge
Hoechst
TFE3
Merge
Veh
Torin-1
Tunicamycin
Chloroquine

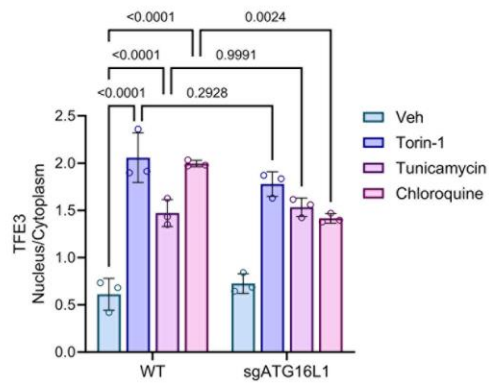
<0.0001
0.0024
<0.0001
0.9991
<0.0001
0.2928
TFE3
Nucleus/Cytoplasm
2.5
2.0
1.5
1.0
0.5
0.0
WT
sgATG16L1
Veh
Torin-1
Tunicamycin
Chloroquine

Figure 25. Golgi stress-specific function of LC3 lipidation in TFE3 regulation.

Confocal images of HeLa sgCtrl and sgATG16L1 cells exposed to 250 nM Torin-1 (1 h), 2 mg/ml tunicamycin (16 h), or 50 μM chloroquine (2 h) and immunostained with anti-TFE3 antibody. Nuclei were stained by Hoechst dye 33342 (top). Scale bar, 10 μm. The nucleus/cytoplasm ratio of TFE3 fluorescence intensity is represented as mean ± s.d. (n = 3, 109 ~ 176 cells per experiment, two-way ANOVA followed by Tukey's multiple comparisons test) (bottom).

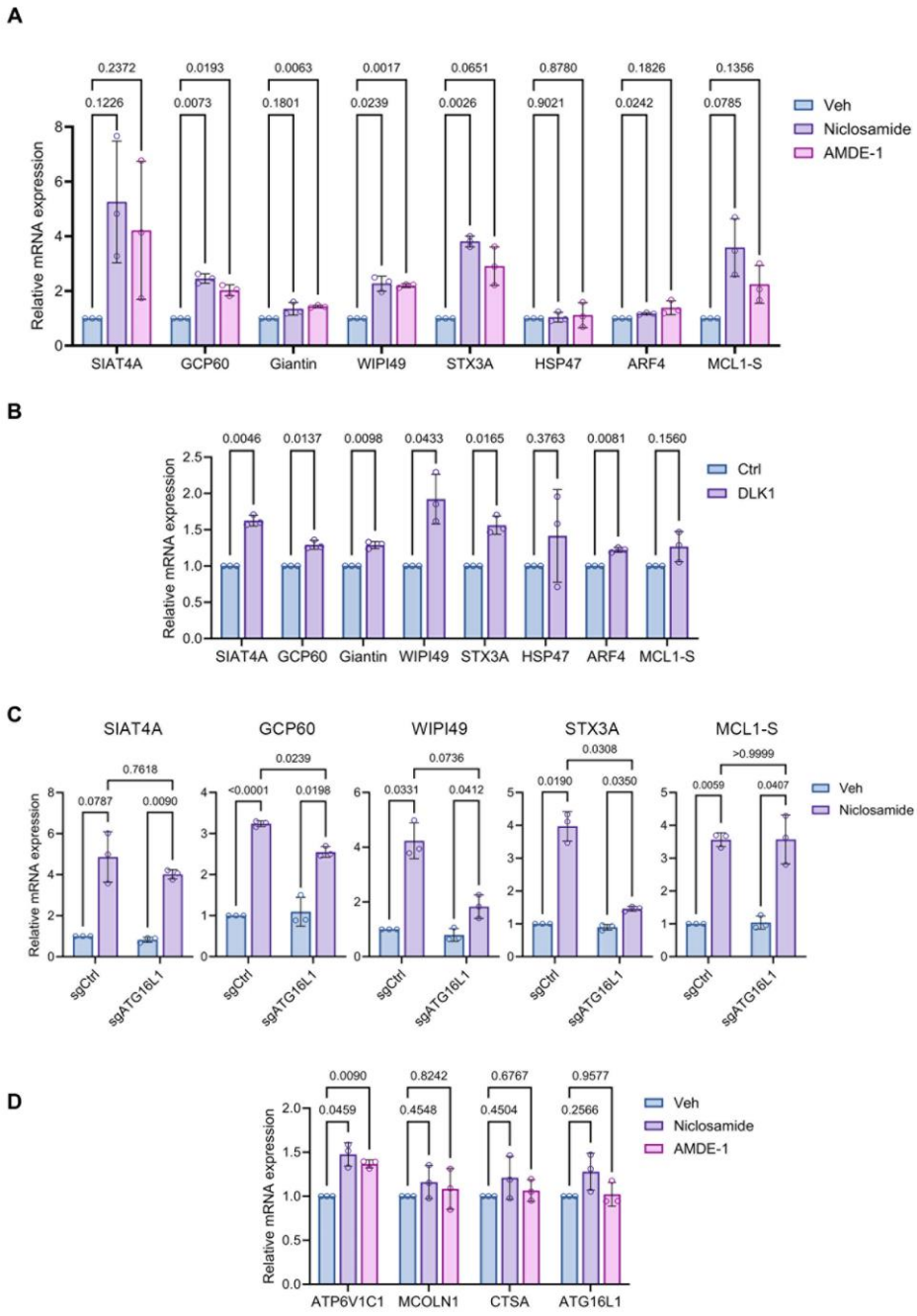
A
Relative mRNA expression
Veh
Niclosamide
AMDE-1
SIAT4A
GCP60
Giantin
WIPI49
STX3A
HSP47
ARF4
MCL1-S
B
Ctrl
DLK1
C
sgCtrl
sgATG16L1
D
ATP6V1C1
MCOLN1
CTSA
ATG16L1

Figure 26. Loss of ATG16L1 abrogates TFE3 target genes upregulation in post-Golgi trafficking inhibition.

(A, B) RNA of HeLa cells exposed to 10 μM niclosamide or 10 μM AMDE-1 for 6 h (A) or expressing pcDNA3-HA (Ctrl) or DLK1-HA (B) was analyzed with quantitative real-time PCR. Bars represent mean ± s.d. (n = 3, one-way ANOVA followed by Dunnett's multiple comparisons test in A, two-tailed Student's t test in B). (C) RNA of HeLa sgCtrl and sgATG16L1 cells exposed to 10 μM niclosamide for 6 h was analyzed with quantitative real-time PCR. Bars represent mean ± s.d. (n = 3, two-way ANOVA followed by Tukey's multiple comparisons test). (D) RNA of HeLa cells exposed to 10 μM niclosamide or 10 μM AMDE-1 for 6 h was analyzed with quantitative real-time PCR. Bars represent mean ± s.d. (n = 3, one-way ANOVA followed by Dunnett's multiple comparisons test).

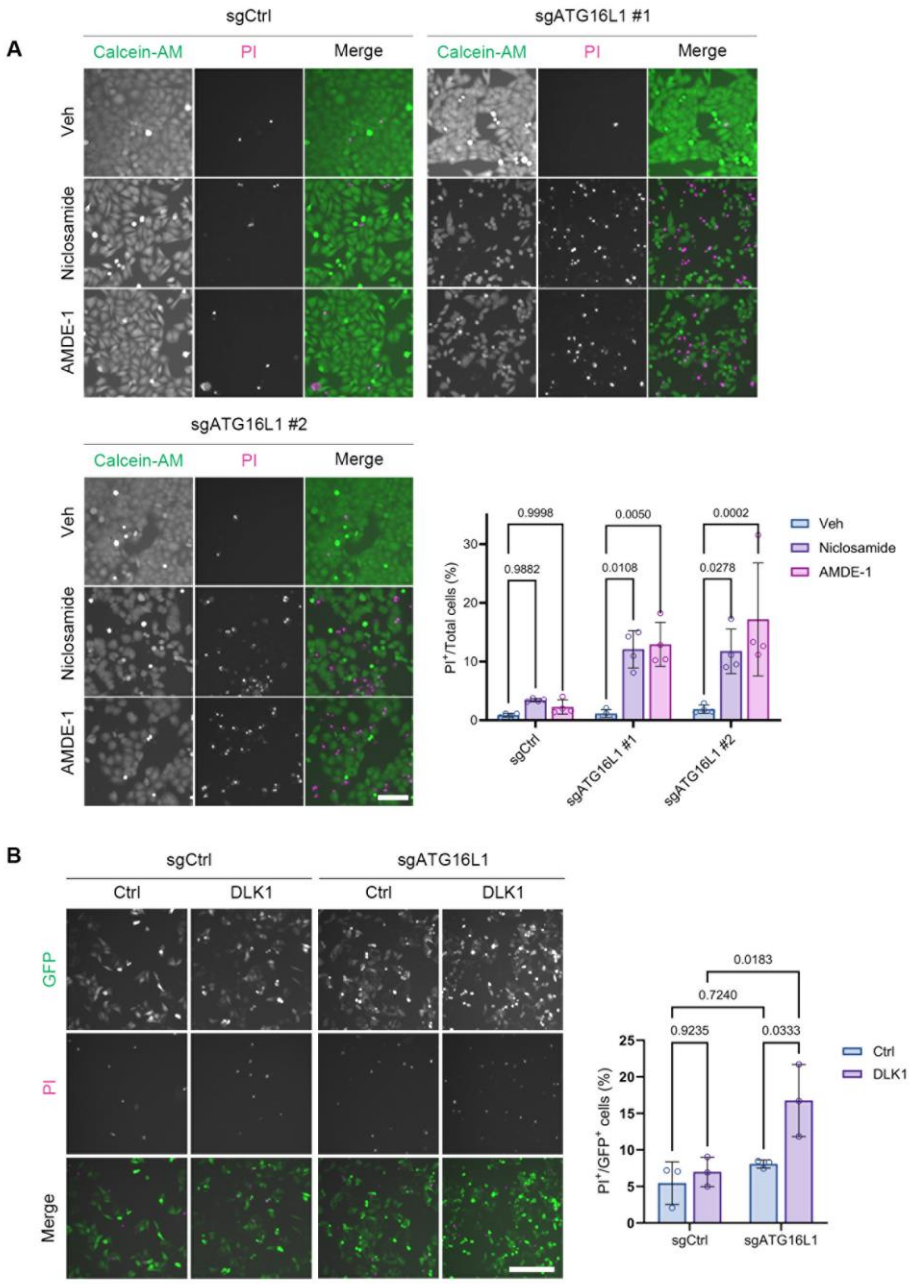
A
sgCtrl
sgATG16L1 #1
sgATG16L1 #2
Calcein-AM
PI
Merge
Veh
Niclosamide
AMDE-1
PI+/Total cells (%)
0.9998
0.9882
0.0050
0.0108
0.0002
0.0278
Veh
Niclosamide
AMDE-1
sgCtrl
sgATG16L1 #1
sgATG16L1 #2
B
sgCtrl
sgATG16L1
Ctrl
DLK1
GFP
PI
Merge
PI+/GFP+ cells (%)
0.0183
0.7240
0.9235
0.0333
Ctrl
DLK1
sgCtrl
sgATG16L1

Figure 27. LC3 lipidation ameliorates Golgi stress-induced cytotoxicity.

(A) HeLa sgCtrl, sgATG16L1 #1, and sgATG16L1 #2 cells were treated with 10 μM niclosamide or 10 μM AMDE-1 for 24 h. After incubation with 1 μM Calcein-AM and 5 μM Propidium Iodide (PI), cells were observed by fluorescence microscopy. Scale bar, 100 μm. The percentages of PI-positive cells are represented as mean ± s.d. (n = 4, 1347 ~ 3517 cells per experiment, two-way ANOVA followed by Tukey's multiple comparisons test) (bottom, right). (B) HeLa sgCtrl, sgATG16L1 cells were co-transfected with EGFP-N1 and pcDNA3-HA (Ctrl) or DLK1-HA for 24 h. After incubation with 5 μM Propidium Iodide (PI), cells were observed by fluorescence microscopy (left). Scale bar, 200 μm. The percentages of PI-positive cells are represented as mean ± s.d. (n = 3, 493 ~ 1255 cells per experiment, two-way ANOVA followed by Tukey's multiple comparisons test) (right).

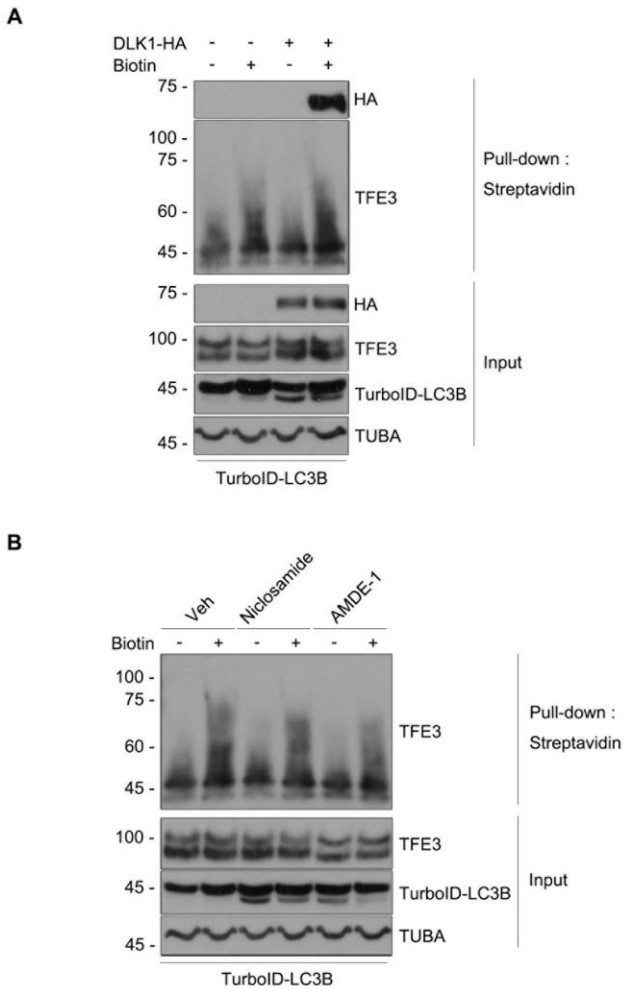
A
DLK1-HA - - + +
Biotin - + - +
75 -
HA
100 -
75 -
60 -
45 -
TFE3
Pull-down :
Streptavidin
75 -
HA
100 -
TFE3
45 -
TurboID-LC3B
45 -
TUBA
Input
TurboID-LC3B
B
Veh
Niclosamide
AMDE-1
Biotin - + - + - +
100 -
75 -
60 -
45 -
TFE3
Pull-down :
Streptavidin
100 -
TFE3
45 -
TurboID-LC3B
45 -
TUBA
Input
TurboID-LC3B

Figure 28. LC3 does not directly binds to TFE3 under Golgi stress.

(A) HeLa cells expressing DLK1-HA and TurboID-LC3B were treated with 100 μM biotin for 6 h, lysed and incubated with streptavidin-agarose beads. Enriched biotinylated proteins (Pull-down: Streptavidin) and whole cell lysates (Input) were analyzed by immunoblotting. (B) HeLa cells expressing TurboID-LC3B were treated with 10 μM niclosamide or 10 μM AMDE-1 together with 100 μM biotin for 6 h, lysed and incubated with streptavidin-agarose beads. Enriched biotinylated proteins (Pull-down: Streptavidin) and whole cell lysates (Input) were analyzed by immunoblotting.

Discussion

In this study, I have found that Golgi-LC3 lipidation facilitates TFE3 nuclear translocation to alleviate Golgi damage from post-Golgi trafficking inhibition. In addition to the previously identified few chemical inducers of Golgi-LC3 lipidation, I have established a genetic model inducing Golgi-specific LC3 lipidation with DLK1 overexpression, which is expected to possibly exclude non-specific effects of the chemical reagents on other organelles than the Golgi apparatus.

Despite increasing reports, it has not been clearly shown what causes Golgi-LC3 lipidation. Here, I believe that dysfunction in post-Golgi trafficking is a common cause of Golgi-LC3 lipidation. Especially, assays utilizing RUSH system in ATG16L1 KO cells allowed me to conclude that LC3 lipidation is a consequence, rather than a cause, of post-Golgi trafficking inhibition. Among several Golgi-LC3 lipidation inducers previously reported, only oleate was shown to inhibit protein secretion from the Golgi apparatus (Cerrato et al., 2021). In my assays employing RUSH system, post-Golgi transport was blocked by DLK1 overexpression or niclosamide and AMDE-1 treatment. However, whether post-Golgi trafficking defects under various Golgi stress conditions are primarily and always associated with Golgi-LC3 lipidation remains elusive.

This study proposes that Golgi-LC3 lipidation under post-Golgi trafficking defects is a Golgi-specific form of CASM based on the following features. First, two ubiquitin-like conjugation systems, but not upstream autophagy regulators, are indispensable for Golgi-LC3 lipidation. Previously, oleate, niclosamide and AMDE-1 were all reported to induce Golgi-LC3 lipidation independently of autophagy regulators, including ULK1 and class Ⅲ phosphatidylinositol 3-kinase (PI3KC3) complex (Gao et al., 2016; Liu et al., 2019; Niso-Santano et al, 2015). Likewise, DLK1 overexpression also induces ULK1/2 and FIP200-independent Golgi-LC3 lipidation. In contrast, molecular machinery involved in LC3-phospholipid conjugation is essential for all types of Golgi-LC3 lipidation. Second, the V-ATPase-ATG16L1 axis, a key molecular feature of CASM which is less studied in Golgi apparatus, is also essential for these Golgi-LC3 lipidation. In Golgi-LC3 lipidation, the ATP6V1A-ATG16L1 interaction is triggered by post-Golgi trafficking inhibition, but is suppressed by bafilomycin A1 and WD40 domain deletion.

Given dysregulation of luminal ion and pH balance is a common cause of diverse CASM types (Durgan & Florey, 2022), I utilized pHluorin-based Golgi pH sensor to examine whether Golgi-LC3 lipidation also can be coupled to ion and pH imbalances. The Golgi apparatus lumen became akalinized only under DLK1 overexpression, with negligible effect of niclosamide and AMDE-1. Therefore, post-Golgi trafficking inhibition is not commonly sensed

and conveyed to V-ATPase-ATG16L1 axis by pH imbalances. This could explain why Golgi pH inhibition by monensin and ammonium chloride are not associated with Golgi-LC3 lipidation (Florey et al, 2015; Li et al, 2016). Post-Golgi trafficking inhibition may prevents post-Golgi distribution of phosphatidyl 4-phosphate (PI(4)P), a phospholipid highly enriched in the *trans*-Golgi network (De Matteis et al, 2013). As PI(4)P is shown to interact with V0 A subunit for Golgi localization of V-ATPase, I could hypothesize that PI(4)P accumulation on the Golgi apparatus could increase V0-V1 assembly at the Golgi apparatus, leading to Golgi-LC3 lipidation via ATG16L1 recruitment. Actin filaments interact with V1 subunits B2 and C1 to maintain V0-V1 assembly at the Golgi apparatus (Serra-Peinado et al, 2016). Another plausible model is that post-Golgi trafficking enhances actin filament-based V0-V1 assembly at the Golgi apparatus for Golgi-LC3 lipidation.

Autophagy-independent functions of LC3 lipidation in the endolysosomal systems have been characterized in LC3-associated phagocytosis, endocytosis, entosis, extracellular vesicles cargo loading and secretion (Florey et al., 2011; Heckmann et al., 2019; Leidal et al., 2020; Sanjuan et al, 2007). While the role of Golgi-LC3 lipidation under Golgi damage remains still largely elusive, this study reveals that Golgi-LC3 lipidation facilitates TFE3 activation to restore Golgi homeostasis. I propose that LC3 lipidation may function as one of the sensors in the TFE3-mediated Golgi stress response. However, LC3 lipidation is unlikely a sole sensor causing

nuclear translocation of TFE3 as there is also LC3 lipidation-independent TFE3 regulation by brefeldin A and monensin (Taniguchi et al., 2015). Until now, the phosphatase responsible for TFE3 dephosphorylation under Golgi stress has not been identified. As TFE3 does not directly bind to LC3 (Figure. 28), Golgi-LC3 lipidation may activate Golgi stress-specific phosphatases to dephosphorylate TFE3 for its nuclear translocation. Considering TFE3 dephosphorylation by calcineurin under ER stress (Martina et al., 2016) and calcium efflux by LC3 lipidation under lysosomal stress (Nakamura et al., 2020), LC3 lipidation may also be involved in calcium efflux from the Golgi apparatus, leading to TFE3 dephosphorylation via calcineurin.

Structural and functional disturbances of the Golgi apparatus resulting from genetic mutations have been implicated in a range of human diseases, with a significant number of these mutations linked to membrane trafficking from the Golgi apparatus (Liu et al, 2021). Mutations in adaptor protein complex-1 (AP-1) subunits responsible for clathrin-coated vesicles formation at the *trans*-Golgi network and in other post-Golgi trafficking pathways (ARFGEF2, ATP2C1, ATP7, FGD1) cause diverse human diseases (García-Cazorla et al, 2022; Liu et al., 2021; Sanger et al, 2019). I hypothesize that Golgi-LC3 lipidation may be induced by genetic mutations associated with post-Golgi trafficking defects. In future, models of genetic disorders associated with post-Golgi trafficking

inhibition need to be established to further elucidate the pathophysiological role of Golgi-LC3 lipidation and TFE3.

In conclusion, I have shown that Golgi stress related to post-Golgi trafficking induces Golgi-LC3 lipidation via the V-ATPase-ATG16L1 axis and have elucidated the function of LC3 lipidation in TFE3 activation. These findings provide integrative and in-depth mechanism of Golgi-LC3 lipidation and suggest that LC3 lipidation is a sensor of TFE3 pathway in the Golgi stress response.

Materials and methods

Antibodies and reagents

The following primary antibodies were used: anti-DLK1 (sc-376755, Santa Cruz Biotechnology); anti-LC3B (NB100-2220, Novus Biologicals); anti-ATG16L1 (D6D5, Cell Signaling Technology); anti-Golgin-97 (A-21270, Thermo Fischer Scientific); anti-HA (sc-7392, Santa Cruz Biotechnology); anti-Myc (sc-40, Santa Cruz Biotechnology); anti-ACTB (sc-47779, Santa Cruz Biotechnology); anti-GAPDH (sc-47724, Santa Cruz Biotechnology); anti-TUBA (sc-23948, Santa Cruz Biotechnology); anti-ATP6V1A (17115-1-AP, Proteintech); anti-FLAG (F1804, Sigma-Aldrich); anti-TFE3 (A0548, ABclonal); anti-Lamin A/C (sc-376248, Santa Cruz Biotechnology); anti-GM130 (610822, BD Biosciences); anti-TGN46 (A19618, ABclonal); anti-FLAG M2 Affinity Gel (A2220, Sigma-Aldrich). All of the primary antibodies were diluted at 1:3000 for immunoblotting and diluted at 1:100 for immunocytochemistry. The following secondary antibodies were used for immunoblotting: horseradish peroxidase (HRP)-conjugated goat anti-mouse IgG, F(ab')2 fragment specific (115-035-006, Jackson ImmunoResearch); HRP-conjugated goat anti-rabbit IgG, F(ab')2 fragment specific (111-035-006, Jackson ImmunoResearch). The following secondary antibodies were used for immunocytochemistry: goat

anti-mouse IgG (H+L) secondary antibody, Alexa Fluor 488 (A-11001, Thermo Fischer Scientific); goat anti-mouse IgG (H+L) secondary antibody, Alexa Fluor 594 (A-11005, Thermo Fischer Scientific); goat anti-rabbit IgG (H+L) secondary antibody, Alexa Fluor 488 (A-11008, Thermo Fischer Scientific); goat anti-rabbit IgG (H+L) secondary antibody, Alexa Fluor 594 (A-11012, Thermo Fischer Scientific). All of the secondary antibodies were diluted at 1:40000 for immunoblotting and diluted at 1:500 for immunocytochemistry. The following reagents were used: dimethyl sulfoxide (DMSO, D2650, Sigma-Aldrich); biotin (B4501, Sigma-Aldrich); brefeldin A (B7651, Sigma-Aldrich); monensin (M5273, Sigma-Aldrich); niclosamide (N3510, Sigma-Aldrich); AMDE-1 (4N-049, Key Organics); bafilomycin A1 (196000, Sigma-Aldrich); concanamycin A (ab144227, Abcam); chloroquine (C6628, Sigma-Aldrich); Torin-1 (4247, Tocris Bioscience); tunicamycin (T7765, Sigma-Aldrich).

Cell culture and DNA transfection

HeLa, HEK293T cells and MEFs were cultured in Dulbecco's modified Eagle's medium (DMEM, HyClone) supplemented with 10% fetal bovine serum (FBS, Gibco) and 50 μg/ml gentamicin (Gibco) in a 5% CO2 incubator at 37℃. Transfection was performed using Lipofectamine 2000 (Thermo Fischer Scientific) or Lipofector-pMAX (AptaBio) according to the manufacturer's instructions.

Plasmid construction

Human DLK1 cDNA was subcloned into pcDNA3-HA. Human TGOLN2 cDNA was subcloned into pEGFP-N1 and mRFP-N1. Human ATG16L1 cDNA was subcloned into mRFP-C1. EGFP-LC3B G120A and deletion mutants of DLK1 and ATG16L1 were produced by site-directed mutagenesis. Human B4GALT1 cDNA (1-82 amino acids) was subcloned into pME pHluorin2. Human TGOLN2 cDNA and mRFP1 cDNA was subcloned into pEGFP-N1. TurboID-LC3B was generated by replacing Sec61b with LC3B from V5-TurboID-Sec61b. All plasmid constructs were verified by DNA sequencing analysis.

Generation of knockout cell line by CRISPR-Cas9 system

HeLa control cell line and two ATG16L1 knockout cell lines were generated by using independent single guide RNAs (sgRNAs) with following target sequences:

sgCtrl, 5'-ACGGAGGCTAAGCGTCGCAA-3';

sgATG16L1 #1, 5'-ACTGAATTACACAAGAAACG-3';

sgATG16L1 #2, TTGGTGCTTAATCCTCAGTT-3'.

sgRNA constructs were produced by insertion of annealed oligonucleotides into lentiCRISPR v2. Each sgRNA was transfected into HeLa cells using Lipofector-pMAX for 24 h and then cells were incubated with 1 μg/ml puromycin for 48 h. Single clones were isolated by seeding single cell per well in 96-well plates by serial

dilution. Protein expression of ATG16L1 was validated by immunoblotting.

Cell lysis and immunoblotting

Cells were washed with ice-cold PBS and lysed with RIPA buffer (50 mM Tris-Cl pH 8.0, 150 mM NaCl, 1% NP-40, 0.5% sodium deoxycholate, 0.1% SDS) supplemented with protease inhibitor cocktail (Quartett) and phosphatase inhibitors (1 mM Na3VO4, 1 mM NaF). Supernatants were collected by centrifugation at 12,000 g for 10 min at 4℃ and protein concentration was measured using the Bradford assay. The supernatants were mixed with 4X Laemmli buffer (250 mM Tris-Cl pH 6.8, 10% SDS, 20% 2-mercaptoethanol, 40% glycerol, 0.08% bromophenol blue) and heated for 10 min at 95℃. Proteins in cell lysates were separated by SDS-PAGE and transferred to polyvinylidene difluoride (PVDF) membranes. The membranes were blocked with TBST containing 5% bovine serum albumin (BSA, GenDEPOT) for 1 h at room temperature and incubated with primary antibodies overnight at 4℃. After washed three times with TBST, membranes were incubated with secondary antibodies for 1 h at room temperature and further washed four times with TBST. Protein bands were visualized using enhanced chemiluminescence detection method.

Immunoprecipitation

Cells were washed with ice-cold PBS and lysed with lysis buffer (50 mM Tris-Cl pH 7.4, 150 mM NaCl, 1 mM EDTA, 1% Triton X-100) supplemented with protease inhibitor cocktail (Quartett) and phosphatase inhibitors (1 mM Na3VO4, 1 mM NaF). Supernatants were cleared by centrifugation at 12,000 g for 10 min at 4℃ and incubated with anti-FLAG M2 Affinity Gel overnight at 4℃. The gels were washed four times with lysis buffer and eluted with lysis buffer containing 4X Laemmli buffer. After heating for 10 min at 95℃, the immunoprecipitated proteins were analyzed by immunoblotting.

TFE3 phosphorylation assay with Phos-tag SDS-PAGE

Proteins in cell lysates were separated by SDS-PAGE supplemented with Phos-tag acrylamide (FujiFilm Wako) and MnCl2 according to the manufacturer's instructions. The gel was washed once in transfer buffer containing 10 mM EDTA for 10 min, followed by washing in transfer buffer without EDTA for 10 min. Proteins were transferred to PVDF membranes. TFE3 proteins were labeled with primary and secondary antibodies and visualized using enhanced chemiluminescence detection method.

Immunocytochemistry and microscopy

For immunocytochemistry, cells were seeded on coverslips and transfected with plasmids or incubated with chemical reagents as

indicated in the figures. Cells were fixed with 4% paraformaldehyde (Sigma-Aldrich) in PBS for 10 min, permeabilized with 0.1% Triton X-100 in PBS for 10 min and blocked with 4% BSA in PBS-T for 1 h at room temperature. After incubation with primary antibodies diluted in PBS-T with 1% BSA overnight at 4℃, cells were incubated with secondary antibodies in PBS-T with 1% BSA for 1 h at room temperature. Nuclei were stained with 1 μg/ml Hoechst 33342 (Sigma-Aldrich). Coverslips were mounted using Fluoromount aqueous mounting medium (Sigma-Aldrich). Fluorescently labeled samples were observed by confocal laser scanning microscope (Leica TCS SP8) or fluorescence microscope (Olympus IX-50 equipped with CoolLED pE-300white and ProgRes MFcool camera, Jenoptik).

Image processing and quantification

Images were analyzed with Fiji and processed using LAS X Office software and Adobe Photoshop. Pearson's correlation coefficient was quantified by BIOP JACoP in Fiji plugin with a region of interest manually drawn around individual cells. To quantify the subcellular localization of TFE3, nuclear region was determined by Hoechst staining and the cytoplasmic region was determined by excluding nuclear region from the entire cellular region. Mean fluorescence intensity of TFE3 in nuclear and cytoplasmic region was measured and the ratio was calculated. For each independent experiment, numerical values obtained from individual cells were averaged and

the mean values were represented as individual symbols on the graphs.

Retention using selective hoos (RUSH) system

For protein trafficking assay under DLK1 overexpression, HeLa cells were transfected with pcDNA3-HA or DLK1-HA together with Str-KDEL_SBP-EGFP-GPI for 24 h and further treated with or without 100 μM biotin for 2 h. For protein trafficking assay under niclosamide and AMDE-1 incubation, HeLa cells were transfected with Str-KDEL_SBP-EGFP-GPI for 24 h and treated with 10 μM niclosamide or 10 μM AMDE-1 for 4 h and further treated together with or without 100 μM biotin for 2 h. Cells were immunostained with anti-Golgin-97 antibody and imaged by fluorescence microscope. The percentages of cells with post-Golgi trafficking inhibition were calculated by dividing the number of cells with EGFP-GPI accumulation at the region of Golgin-97 by the number of EGFP-GPI-expressing cells. In Fig. 3d,g, the percentages of cells showing EGFP-GPI accumulation at perinuclear region were calculated to determine post-Golgi trafficking inhibition.

Nuclear and cytoplasmic fractionation

Cells were lysed in fractionation buffer (20 mM HEPES pH 7.4, 10 mM KCl, 2 mM MgCl2, 1 mM EDTA, 1 mM EGTA, 1 mM DTT) supplemented with protease inhibitor cocktail (Quartett) and phosphatase inhibitors (1 mM Na3VO4, 1 mM NaF) by suspending

through 1 ml syringe with a 26 gauge needle. After 20 min, a portion of cell lysates were collected as whole cell lysate (WCL) fraction and remaining cell lysates were centrifugated at 720 g for 5 min at 4℃. The pellet represented nuclear fraction and was washed twice with fractionation buffer, lysed in RIPA buffer containing 4X Laemmli buffer. The supernatant represented the cytoplasmic fraction and was cleared by centrifugation at 12,000 g for 10 min at 4℃, mixed with 4X Laemmli buffer. Cytoplasmic, nuclear fraction and WCL were analyzed by immunoblotting.

RNA extraction and reverse transcription quantitative real-time PCR

Total RNA was extracted using TRIzol reagent (Molecular Research Center) according to the manufacturer's instructions. Complementary DNA was generated using Moloney murine leukemia virus reverse transcriptase (M-MLV RT, Enzynomics) and Oligo (dT)18 primer (GenDEPOT). Quantitative real-time PCR was performed using Power SYBR Green PCR Master Mix (Applied Biosystems) on QuantStudio 3 real-time PCR system (Applied Biosystems). Target gene expression was normalized to GAPDH. The primer sequences were as follows:

SIAT4A (forward), 5'-GGA GGA CGA CAC CTA CCG AT-3'; SIAT4A (reverse), 5'-CCA CCG ACC TCT TCT CCA G-3'; GCP60 (forward), 5'-AGC GTG CAT GTC AGT GAG TCC-3'; GCP60 (reverse), 5'-GGC ACA ATC TCA TCC AGC AAA G-3'; Giantin

(forward), 5'-CAC TCA GGA GCA GGC ACT GTT A-3'; Giantin (reverse), 5'-CAG GAC TCG CTT CCA TCC AA-3'; WIPI49 (forward), 5'-AGT CAG TCA CAC AAA ACC ACG-3'; WIPI49 (reverse), 5'-AGA GCA CAT AGA CCT GTT GGG-3'; STX3A (forward), 5'-TCG GCA GAC CTT CGG ATT C-3'; STX3A (reverse), 5'-TCC TCA TCG GTT GTC TTT TTG C-3'; HSP47 (forward), 5'-AAG AGC AGC TGA AGA TCT GGA TG-3'; HSP47 (reverse), 5'-GTC GGC CTT GTT CTT GTC AAT G-3'; ARF4 (forward), 5'-GAG ATA GTC ACC ACC ATT CCT ACC A-3'; ARF4 (reverse), 5'-GGC CTA ATT CTA TCT TGA CCA CCA-3'; MCL1-S (forward), 5'-GGC CTT CCA AGG ATG GGT TT-3'; MCL1-S (reverse), 5'-ACT CCA GCA ACA CCT GCA AAA-3'; ATP6V1C1 (forward), 5'-GAG TTC TGG CTT ATA TCT GCT CC-3'; ATP6V1C1 (reverse), 5'-GTG CCA ACC TTT AAG TCA GGA AT-3'; MCOLN1 (forward), 5'-TTG CTC TCT GCC AGC GGT ACT A-3'; MCOLN1 (reverse), 5'-GCA GTC AGT AAC CAC CAT CGG A-3'; CTSA (forward), 5'-CAG GCT TTG GTC TTC TCT CCA-3'; CTSA (reverse), 5'-TCA CGC ATT CCA GGT CTT TG-3'; ATG16L1 (forward), 5'-CAG TTA CGT GGC GGC AGG CT-3'; ATG16L1 (reverse), 5'-ACA ACG TGC GAG CCA GAG GG-3'; GAPDH (forward), 5'-AGA AGG CTG GGG CTC ATT TG-3'; GAPDH (reverse), 5'-AGG GGC CAT CCA CAG TCT TC-3'.

Cell viability assay

Dead cells were stained with 5 μM propidium iodide (PI, Sigma-Aldrich) and viable cells were stained with 1 μM calcein-AM (Thermo Fischer Scientific). Cells were observed by fluorescence microscope. Cell viability was calculated by dividing the number of PI-positive cells by the number of total cells (calcein-AM-positive cells plus PI-positive).

Proximity labeling experiments

For LC3B-proximal protein labeling under DLK1 overexpression, HeLa cells were transfected with pcDNA3-HA or DLK1-HA together with TurboID-LC3B for 24 h and further treated with 100 μM biotin for 6 h. For LC3B-proximal protein labeling under niclosamide and AMDE-1 incubation, HeLa cells were transfected with TurboID-LC3B for 24 h and treated with 10 μM niclosamide or 10 μM AMDE-1 together with 100 μM biotin for 6 h. Cells were washed three times with ice-cold PBS to stop the labeling reaction and lysed with RIPA buffer supplemented with protease inhibitor cocktail (Quartett). Supernatants were cleared by centrifugation at 12,000 g for 10 min at 4℃ and incubated with streptavidin-agarose conjugate (Millipore) overnight at 4℃. The beads were washed four times with RIPA buffer and eluted with RIPA buffer containing 4X Laemmli buffer. After heating for 10 min at 95℃, the purified biotinylated proteins were analyzed by immunoblotting.

Transmission electron microscopy.

Cells were fixed with Karnovsky's fixative buffer and washed three times with 0.05 M sodium cacodylate buffer. Postfixation was performed with 1% osmium tetroxide in 0.1 M sodium cacodylate buffer. Cells were washed three times with distilled water, stained with 0.5% uranyl acetate, further washed three times with distilled water. After serial dehydration with increasing concentration of ethanol, cells were transiently embedded in Spurr's resin. Ultrathin sections were obtained and observed using JEM1010 transmission electron microscope (JEOL).

Flow cytometry for Golgi pH measure

For Golgi pH measure under DLK1 overexpression, HeLa cells were transfected with pcDNA3-HA, DLK1-HA or DLK1-HA isoform 2 together with GALT-pH2 for 24 h. For Golgi pH measure under niclosamide and AMDE-1 incubation, HeLa cells were transfected with GALT-pH2 for 24 h and treated with 10 μM niclosamide or 10 μM AMDE-1 for 6 h. Cells were washed twice with PBS and incubated with trypsin-EDTA. Trypsinized cells were washed and resuspended with Hank's balanced salt solution buffer supplemented with 1.5 mM $CaCl_2$, 10 mM HEPES, 5% fetal bovine serum and 5.55 mM glucose. Flow cytometry was performed using Flow Activated Cell Sorter cantoII. Non-transfected cells were also sorted and the 405/488 excitation ratio was analyzed in cells exhibiting fluorescence signals.

Statistics and reproducibility

All experiments were independently repeated at least three times and quantitative data are represented as the mean ± standard deviation (s.d.). Statistical analyses were performed using GraphPad Prism 10 and calculated P values are described in figures. No statistical methods were used to predetermine the sample sizes. The number of biologically independent experiments and type of statistical test are indicated in the figure legends. Comparison between two groups was determined by two-tailed Student's t test. Data from three or more groups with one independent variable were compared by one-way ANOVA followed by Dunnett's or Tukey's multiple comparisons test. Data from two independent variables were compared by two-way ANOVA followed by Tukey's multiple comparisons test. Comparison of relative protein level from immunoblot data and relative mRNA expression from real-time PCR data was determined by repeated measures one-way or two-way ANOVA using Geisser-Greenhouse correction, followed by Dunnett's or Tukey's multiple comparisons test.

References

Baladrón V, Ruiz-Hidalgo MJ, Nueda ML, Díaz-Guerra MJ, García-Ramírez JJ, Bonvini E, Gubina E, Laborda J (2005) dlk acts as a negative regulator of Notch1 activation through interactions with specific EGF-like repeats. Exp Cell Res 303: 343-359

Baumann J, Ignashkova TI, Chirasani SR, Ramírez-Peinado S, Alborzinia H, Gendarme M, Kuhnigk K, Kramer V, Lindemann RK, Reiling JH (2018) Golgi stress-induced transcriptional changes mediated by MAPK signaling and three ETS transcription factors regulate MCL1 splicing. Mol Biol Cell 29: 42-52

Benyair R, Eisenberg-Lerner A, Merbl Y (2022) Maintaining Golgi Homeostasis: A Balancing Act of Two Proteolytic Pathways. Cells 11

Boncompain G, Divoux S, Gareil N, de Forges H, Lescure A, Latreche L, Mercanti V, Jollivet F, Raposo G, Perez F (2012) Synchronization of secretory protein traffic in populations of cells. Nat Methods 9: 493-498

Cerrato G, Leduc M, Müller K, Liu P, Zhao L, Humeau J, Xie W, Zhang S, Kepp O, Sauvat A et al (2021) Oleate-induced

aggregation of LC3 at the trans-Golgi network is linked to a protein trafficking blockade. Cell Death Differ 28: 1733-1752

Chang HY, Yang WY (2022) Golgi quality control and autophagy. IUBMB Life 74: 361-370

D'Souza B, Meloty-Kapella L, Weinmaster G (2010) Canonical and non-canonical Notch ligands. Curr Top Dev Biol 92: 73-129

De Matteis MA, Wilson C, D'Angelo G (2013) Phosphatidylinositol-4-phosphate: the Golgi and beyond. Bioessays 35: 612-622

Dinter A, Berger EG (1998) Golgi-disturbing agents. Histochem Cell Biol 109: 571-590

Durgan J, Florey O (2022) Many roads lead to CASM: Diverse stimuli of noncanonical autophagy share a unifying molecular mechanism. Sci Adv 8: eabo1274

Durgan J, Lystad AH, Sloan K, Carlsson SR, Wilson MI, Marcassa E, Ulferts R, Webster J, Lopez-Clavijo AF, Wakelam MJ et al (2021) Non-canonical autophagy drives alternative ATG8 conjugation to phosphatidylserine. Mol Cell 81: 2031-2040.e2038

Eisenberg-Lerner A, Benyair R, Hizkiahou N, Nudel N, Maor R, Kramer MP, Shmueli MD, Zigdon I, Cherniavsky Lev M, Ulman A et al (2020) Golgi organization is regulated by proteasomal degradation. Nat Commun 11: 409

Falix FA, Aronson DC, Lamers WH, Gaemers IC (2012) Possible roles of DLK1 in the Notch pathway during development and disease. Biochim Biophys Acta 1822: 988-995

Fischer TD, Wang C, Padman BS, Lazarou M, Youle RJ (2020) STING induces LC3B lipidation onto single-membrane vesicles via the V-ATPase and ATG16L1-WD40 domain. J Cell Biol 219

Fletcher K, Ulferts R, Jacquin E, Veith T, Gammoh N, Arasteh JM, Mayer U, Carding SR, Wileman T, Beale R et al (2018) The WD40 domain of ATG16L1 is required for its non-canonical role in lipidation of LC3 at single membranes. Embo j 37

Florey O, Gammoh N, Kim SE, Jiang X, Overholtzer M (2015) V-ATPase and osmotic imbalances activate endolysosomal LC3 lipidation. Autophagy 11: 88-99

Florey O, Kim SE, Sandoval CP, Haynes CM, Overholtzer M (2011) Autophagy machinery mediates macroendocytic processing and

entotic cell death by targeting single membranes. Nat Cell Biol 13: 1335–1343

Fujita N, Itoh T, Omori H, Fukuda M, Noda T, Yoshimori T (2008) The Atg16L complex specifies the site of LC3 lipidation for membrane biogenesis in autophagy. Mol Biol Cell 19: 2092–2100

Gammoh N (2020) The multifaceted functions of ATG16L1 in autophagy and related processes. J Cell Sci 133

Gao J, Gao A, Liu W, Chen L (2021) Golgi stress response: A regulatory mechanism of Golgi function. Biofactors 47: 964–974

Gao Y, Liu Y, Hong L, Yang Z, Cai X, Chen X, Fu Y, Lin Y, Wen W, Li S et al (2016) Golgi-associated LC3 lipidation requires V-ATPase in noncanonical autophagy. Cell Death Dis 7: e2330

García-Cazorla A, Oyarzábal A, Saudubray JM, Martinelli D, Dionisi-Vici C (2022) Genetic disorders of cellular trafficking. Trends Genet 38: 724–751

Gomes-da-Silva LC, Jimenez AJ, Sauvat A, Xie W, Souquere S, Divoux S, Storch M, Sveinbjørnsson B, Rekdal Ø, Arnaut LG et al (2019) Recruitment of LC3 to damaged Golgi apparatus. Cell Death Differ 26: 1467–1484

Goodwin JM, Walkup WGt, Hooper K, Li T, Kishi-Itakura C, Ng A, Lehmberg T, Jha A, Kommineni S, Fletcher K et al (2021) GABARAP sequesters the FLCN-FNIP tumor suppressor complex to couple autophagy with lysosomal biogenesis. Sci Adv 7: eabj2485

Grassi ES, Pietras A (2022) Emerging Roles of DLK1 in the Stem Cell Niche and Cancer Stemness. J Histochem Cytochem 70: 17-28

Grinde B (1983) Effect of carboxylic ionophores on lysosomal protein degradation in rat hepatocytes. Exp Cell Res 149: 27-35

Heckmann BL, Teubner BJW, Tummers B, Boada-Romero E, Harris L, Yang M, Guy CS, Zakharenko SS, Green DR (2019) LC3-Associated Endocytosis Facilitates β-Amyloid Clearance and Mitigates Neurodegeneration in Murine Alzheimer's Disease. Cell 178: 536-551.e514

Hickey KL, Swarup S, Smith IR, Paoli JC, Miguel Whelan E, Paulo JA, Harper JW (2023) Proteome census upon nutrient stress reveals Golgiphagy membrane receptors. Nature 623: 167-174

Homewood CA, Warhurst DC, Peters W, Baggaley VC (1972) Lysosomes, pH and the anti-malarial action of chloroquine. Nature 235: 50-52

Hooper KM, Jacquin E, Li T, Goodwin JM, Brumell JH, Durgan J, Florey O (2022) V-ATPase is a universal regulator of LC3-associated phagocytosis and non-canonical autophagy. J Cell Biol 221

Ichimura Y, Kirisako T, Takao T, Satomi Y, Shimonishi Y, Ishihara N, Mizushima N, Tanida I, Kominami E, Ohsumi M et al (2000) A ubiquitin-like system mediates protein lipidation. Nature 408: 488-492

Jacomin AC, Samavedam S, Promponas V, Nezis IP (2016) iLIR database: A web resource for LIR motif-containing proteins in eukaryotes. Autophagy 12: 1945-1953

Jamaludin MI, Wakabayashi S, Taniguchi M, Sasaki K, Komori R, Kawamura H, Takase H, Sakamoto M, Yoshida H (2019) MGSE Regulates Crosstalk from the Mucin Pathway to the TFE3 Pathway of the Golgi Stress Response. Cell Struct Funct 44: 137-151

Kabeya Y, Mizushima N, Ueno T, Yamamoto A, Kirisako T, Noda T, Kominami E, Ohsumi Y, Yoshimori T (2000) LC3, a mammalian homologue of yeast Apg8p, is localized in autophagosome membranes after processing. Embo j 19: 5720-5728

Kim WK, Choi W, Deshar B, Kang S, Kim J (2023) Golgi Stress Response: New Insights into the Pathogenesis and Therapeutic Targets of Human Diseases. Mol Cells 46: 191-199

Kimura S, Noda T, Yoshimori T (2007) Dissection of the autophagosome maturation process by a novel reporter protein, tandem fluorescent-tagged LC3. Autophagy 3: 452-460

Klionsky DJ, Abdel-Aziz AK, Abdelfatah S, Abdellatif M, Abdoli A, Abel S, Abeliovich H, Abildgaard MH, Abudu YP, Acevedo-Arozena A et al (2021) Guidelines for the use and interpretation of assays for monitoring autophagy (4th edition)(1). Autophagy 17: 1-382

Kumar S, Jain A, Choi SW, da Silva GPD, Allers L, Mudd MH, Peters RS, Anonsen JH, Rusten TE, Lazarou M et al (2020) Mammalian Atg8 proteins and the autophagy factor IRGM control mTOR and TFEB at a regulatory node critical for responses to pathogens. Nat Cell Biol 22: 973-985

Leidal AM, Huang HH, Marsh T, Solvik T, Zhang D, Ye J, Kai F, Goldsmith J, Liu JY, Huang YH et al (2020) The LC3-conjugation machinery specifies the loading of RNA-binding proteins into extracellular vesicles. Nat Cell Biol 22: 187-199

Li Z, Ji X, Wang W, Liu J, Liang X, Wu H, Liu J, Eggert US, Liu Q, Zhang X (2016) Ammonia Induces Autophagy through Dopamine Receptor D3 and MTOR. PLoS One 11: e0153526

Liu J, Huang Y, Li T, Jiang Z, Zeng L, Hu Z (2021) The role of the Golgi apparatus in disease (Review). Int J Mol Med 47

Liu Y, Luo X, Shan H, Fu Y, Gu Q, Zheng X, Dai Q, Xia F, Zheng Z, Liu P et al (2019) Niclosamide Triggers Non-Canonical LC3 Lipidation. Cells 8

Macedo DB, Kaiser UB (2019) DLK1, Notch Signaling and the Timing of Puberty. Semin Reprod Med 37: 174-181

Mahon MJ (2011) pHluorin2: an enhanced, ratiometric, pH-sensitive green florescent protein. Adv Biosci Biotechnol 2: 132-137

Martina JA, Diab HI, Brady OA, Puertollano R (2016) TFEB and TFE3 are novel components of the integrated stress response. Embo j 35: 479-495

Martina JA, Diab HI, Lishu L, Jeong AL, Patange S, Raben N, Puertollano R (2014) The nutrient-responsive transcription factor

TFE3 promotes autophagy, lysosomal biogenesis, and clearance of cellular debris. Sci Signal 7: ra9

Martina JA, Puertollano R (2018) Protein phosphatase 2A stimulates activation of TFEB and TFE3 transcription factors in response to oxidative stress. J Biol Chem 293: 12525–12534

Miyata S, Mizuno T, Koyama Y, Katayama T, Tohyama M (2013) The endoplasmic reticulum–resident chaperone heat shock protein 47 protects the Golgi apparatus from the effects of O–glycosylation inhibition. PLoS One 8: e69732

Mizushima N (2020) The ATG conjugation systems in autophagy. Curr Opin Cell Biol 63: 1–10

Mizushima N, Kuma A, Kobayashi Y, Yamamoto A, Matsubae M, Takao T, Natsume T, Ohsumi Y, Yoshimori T (2003) Mouse Apg16L, a novel WD–repeat protein, targets to the autophagic isolation membrane with the Apg12–Apg5 conjugate. J Cell Sci 116: 1679–1688

Nakamura S, Shigeyama S, Minami S, Shima T, Akayama S, Matsuda T, Esposito A, Napolitano G, Kuma A, Namba–Hamano T et al (2020) LC3 lipidation is essential for TFEB activation during the

lysosomal damage response to kidney injury. Nat Cell Biol 22: 1252–1263

Nezich CL, Wang C, Fogel AI, Youle RJ (2015) MiT/TFE transcription factors are activated during mitophagy downstream of Parkin and Atg5. J Cell Biol 210: 435–450

Niso-Santano M, Malik SA, Pietrocola F, Bravo-San Pedro JM, Mariño G, Cianfanelli V, Ben-Younès A, Troncoso R, Markaki M, Sica V et al (2015) Unsaturated fatty acids induce non-canonical autophagy. Embo j 34: 1025–1041

Nthiga TM, Shrestha BK, Bruun JA, Larsen KB, Lamark T, Johansen T (2021) Regulation of Golgi turnover by CALCOCO1–mediated selective autophagy. J Cell Biol 220

Peña-Martinez C, Rickman AD, Heckmann BL (2022) Beyond autophagy: LC3–associated phagocytosis and endocytosis. Sci Adv 8: eabn1702

Raggo C, Rapin N, Stirling J, Gobeil P, Smith-Windsor E, O'Hare P, Misra V (2002) Luman, the cellular counterpart of herpes simplex virus VP16, is processed by regulated intramembrane proteolysis. Mol Cell Biol 22: 5639–5649

Reiling JH, Olive AJ, Sanyal S, Carette JE, Brummelkamp TR, Ploegh HL, Starnbach MN, Sabatini DM (2013) A CREB3–ARF4 signalling pathway mediates the response to Golgi stress and susceptibility to pathogens. Nat Cell Biol 15: 1473–1485

Roczniak–Ferguson A, Petit CS, Froehlich F, Qian S, Ky J, Angarola B, Walther TC, Ferguson SM (2012) The transcription factor TFEB links mTORC1 signaling to transcriptional control of lysosome homeostasis. Sci Signal 5: ra42

Sanger A, Hirst J, Davies AK, Robinson MS (2019) Adaptor protein complexes and disease at a glance. J Cell Sci 132

Sanjuan MA, Dillon CP, Tait SW, Moshiach S, Dorsey F, Connell S, Komatsu M, Tanaka K, Cleveland JL, Withoff S et al (2007) Toll–like receptor signalling in macrophages links the autophagy pathway to phagocytosis. Nature 450: 1253–1257

Sanjuan MA, Dillon CP, Tait SW, Moshiach S, Dorsey F, Connell S, Komatsu M, Tanaka K, Cleveland JL, Withoff S et al (2007) Toll–like receptor signalling in macrophages links the autophagy pathway to phagocytosis. Nature 450: 1253–1257

Sasaki K, Komori R, Taniguchi M, Shimaoka A, Midori S, Yamamoto M, Okuda C, Tanaka R, Sakamoto M, Wakabayashi S et al (2019)

PGSE Is a Novel Enhancer Regulating the Proteoglycan Pathway of the Mammalian Golgi Stress Response. Cell Struct Funct 44: 1-19

Schmidt O, Weyer Y, Baumann V, Widerin MA, Eising S, Angelova M, Schleiffer A, Kremser L, Lindner H, Peter M et al (2019) Endosome and Golgi-associated degradation (EGAD) of membrane proteins regulates sphingolipid metabolism. Embo j 38: e101433

Schwabl S, Teis D (2022) Protein quality control at the Golgi. Curr Opin Cell Biol 75: 102074

Serra-Peinado C, Sicart A, Llopis J, Egea G (2016) Actin Filaments Are Involved in the Coupling of V0-V1 Domains of Vacuolar H+-ATPase at the Golgi Complex. J Biol Chem 291: 7286-7299

Smas CM, Green D, Sul HS (1994) Structural characterization and alternate splicing of the gene encoding the preadipocyte EGF-like protein pref-1. Biochemistry 33: 9257-9265

Sønder SL, Häger SC, Heitmann ASB, Frankel LB, Dias C, Simonsen AC, Nylandsted J (2021) Restructuring of the plasma membrane upon damage by LC3-associated macropinocytosis. Sci Adv 7

Tanida I, Ueno T, Kominami E (2004) Human light chain 3/MAP1LC3B is cleaved at its carboxyl-terminal Met121 to expose

Gly120 for lipidation and targeting to autophagosomal membranes. J Biol Chem 279: 47704–47710

Taniguchi M, Nadanaka S, Tanakura S, Sawaguchi S, Midori S, Kawai Y, Yamaguchi S, Shimada Y, Nakamura Y, Matsumura Y et al (2015) TFE3 is a bHLH–ZIP–type transcription factor that regulates the mammalian Golgi stress response. Cell Struct Funct 40: 13–30

Taniguchi M, Yoshida H (2017) TFE3, HSP47, and CREB3 Pathways of the Mammalian Golgi Stress Response. Cell Struct Funct 42: 27–36

Ulferts R, Marcassa E, Timimi L, Lee LC, Daley A, Montaner B, Turner SD, Florey O, Baillie JK, Beale R (2021) Subtractive CRISPR screen identifies the ATG16L1/vacuolar ATPase axis as required for non–canonical LC3 lipidation. Cell Rep 37: 109899

Viotti C (2016) ER to Golgi–Dependent Protein Secretion: The Conventional Pathway. Methods Mol Biol 1459: 3–29

Xu Y, Zhou P, Cheng S, Lu Q, Nowak K, Hopp AK, Li L, Shi X, Zhou Z, Gao W et al (2019) A Bacterial Effector Reveals the V–ATPase–ATG16L1 Axis that Initiates Xenophagy. Cell 178: 552–566.e520

Yamaguchi H, Arakawa S, Kanaseki T, Miyatsuka T, Fujitani Y, Watada H, Tsujimoto Y, Shimizu S (2016) Golgi membrane-associated degradation pathway in yeast and mammals. Embo j 35: 1991-2007

국문초록

ATG8/LC3 단백질은 지질화되어 이중막 구조의 자가포식소체 뿐만 아니라 엔도솜과 라이소좀 등의 단일막 구조의 막에 위치하여 이러한 막 구조 소기관의 기능을 지원할 수 있다. 최신 연구에서 여러 종류의 골지체 손상을 유발하는 조건들에서 LC3 지질화가 골지체 막에서도 발생하는 현상들이 보고되었으나 골지체-LC3 지질화의 분자 기전과 생물학적 기능은 아직 밝혀지지 않았다.

본 연구에서는 골지체 특이적인 LC3 지질화의 새로운 연구 방법으로 DLK1 과발현 조건을 정립하였다. DLK1 과발현 조건에 더해 골지체 손상을 유발하는 두 종류의 화합물인 niclosamide 와 AMDE-1 을 이용하여 골지체-LC3 지질화의 기전과 역할을 밝혔다. DLK1 과발현은 자가포식작용에서 유비퀴틴 유사체 결합 체계로 기능하는 ATG12-ATG5-ATG16L1 복합체를 통해 *trans*-Golgi network 에서의 LC3 단백질의 지질화를 유도한다. 자가포식작용 경로의 상위 조절자인 ULK1/2 와 FIP200 는 DLK1 에 의한 LC3 지질화에 관여하지 않는다. 본 연구에서 골지체 이후 단백질 수송 과정의 억제가 DLK1 과발현 조건뿐만 아니라 niclosamide/AMDE-1 에 의해 유도되는 골지체-LC3 지질화의 공통적인 원인임을 밝혔다. 골지체-LC3 지질화는 ATG16L1 의 WD40 영역과 V 형 ATP 가수분해효소의 상호작용을 통해 ATG16L1 의 골지체로 이동이 선행되어야 한다. 골지체 이후 단백질 수송 과정의 억제는 골지 스트레스 반응의 주요 전사 조절자인 TFE3 를 핵으로 이동시켜 골지 스트레스 반응의 대상 유전자들의 발현을 증가시킨다. LC3 지질화가 되지 못할 경우 골지체 기능장애에 의해 TFE3 가 핵으로 이동하는

현상이 저해되어 골지 스트레스 반응이 정상적으로 작동되지 못한다. 종합적으로 본 연구는 골지체-LC3 지질화의 분자 기전과 골지 스트레스 반응에서의 새로운 기능을 밝혔다.

주요어: 골지체, LC3 지질화, DLK1, 골지체 이후 수송, V 형 ATP 가수분해효소, 골지 스트레스 반응

학번: 2016-20373